CHAPTER IV
RESULTS AND DISCUSSION

4.1 Tin

The catalytic dehydration of ethanol process consists two main competitive pathways as shown in Figure 2.1. The first reaction is the intermolecular dehydration of ethanol to diethyl ether. The formation of diethyl ether is exothermic and favored between 150 C° and 300 C°. The second reaction is the intramolecular dehydration of ethanol to ethylene which its formation is favored above 300 C° up to 500 C°. Moreover, diethyl ether and ethylene could undergo further reaction to C4 olefins, paraffins and aromatics (BTX) by oligomerization, cracking, cyclization, dehydrogenation and H-transfer (Inaba *et al.*, 2006). SAPO-34 has been employed as solid acid catalyst for ethanol conversion to light olefins. Incorporation of an oxide into SAPO-34 could strongly influence on catalyst behavior in ethanol dehydration.

In this work, the effects of metal oxides, namely tin and antimony oxides with different oxidation states with and without supports on the product distributions of the catalytic dehydration of bio-ethanol were studied. Therefore, this chapter is divided into two main parts, which are tin and antimony. First part, the pure different oxidation states of tin and SnO_x-loaded catalysts are discussed. Second part, the pure antimony with different oxidation states, as well as, Sb_2O_x-loaded catalysts are discussed. The changes of oxidation states of metal oxide were observed as a function of time-on-stream. Table 4.1 summarizes the catalyst names and their nomenclatures.

Table 4.1 Catalysts and their nomenclatures

No.	Catalyst	Calcination Temperature (°C)	Abbreviation
1	SAPO-34	-	SA34
2	5% metallic tin/SAPO-34	400	Sn0SAPO34
3	5% metallic antimony/SAPO-34	400	Sb0SAPO34
4	5%tin oxide/SAPO-34	400	5SnSA34-400
5	7%tin oxide/SAPO-34	400	7SnSA34-400
6	5%antimony oxide/SAPO-34	400	5SnSA34-400
7	7%tin oxide/SAPO-34	400	7SnSA34-400
8	5%tin oxide/SAPO-34	700	5SnSA34-700
9	7%tin oxide/SAPO-34	700	7SnSA34-700
10	5%antimony oxide/SAPO-34	700	5SnSA34-700
11	7%tin oxide/SAPO-34	700	7SnSA34-700

4.1.1 Pure Oxidation States of Tin

4.1.1.1 Characterization of Tins

Table 4.2 shows the specific surface area, pore volume and pore diameter of metallic tin, tin (II) oxide and tin (IV) oxide determined by using Barrett-Joyner-Halenda (BJH) method. As observed in Table 4.2, SnO_2 has higher surface area, pore volume, and pore diameter than SnO and metallic tin. The XRD patterns of commercial metallic tin and tin oxides are displayed in Figure 4.1. The peaks of metallic tin can be detected at $2\theta = 30.6°$, 32.0°, 43.9° and 44.9 °. The peaks of SnO can be observed at $2\theta = 29.8°$, 33.2°, 47.7°, 50.6 and 57.36 ° while the rutile structure of SnO_2 can be mainly detected at $2\theta = 26.5°$, 34° and 51.7°. The XRD patterns confirm the existance of pure oxide phase on each catalyst sample.

Table 4.2 Specific surface area and pore characteristics of tin oxides with different oxidation states

Metal Oxide	BET specific area (m^2/g)	Pore Diameter (nm)	Pore Volume (m^3/g)
Metal Sn	3.7	3.6	0.003
SnO	7.5	5.3	0.01
SnO_2	10.8	15.4	0.04

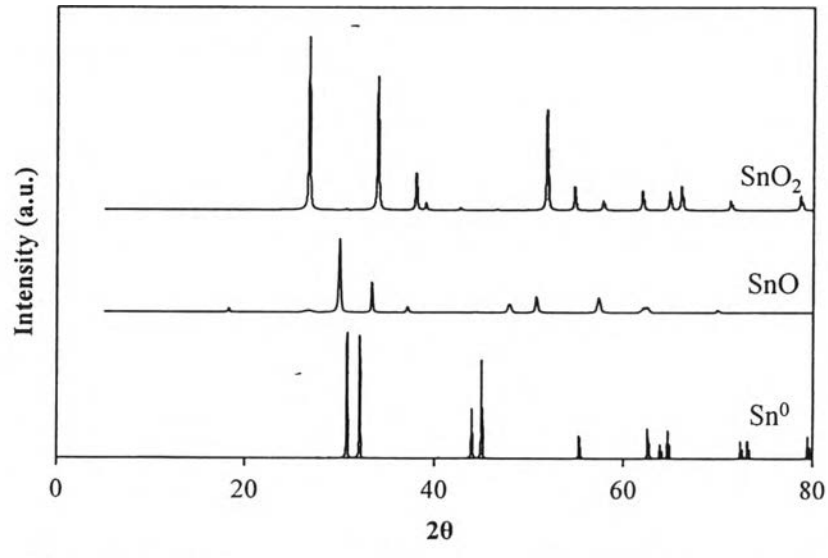

Figure 4.1 X-ray diffraction patterns of fresh tin oxides with different oxidation states.

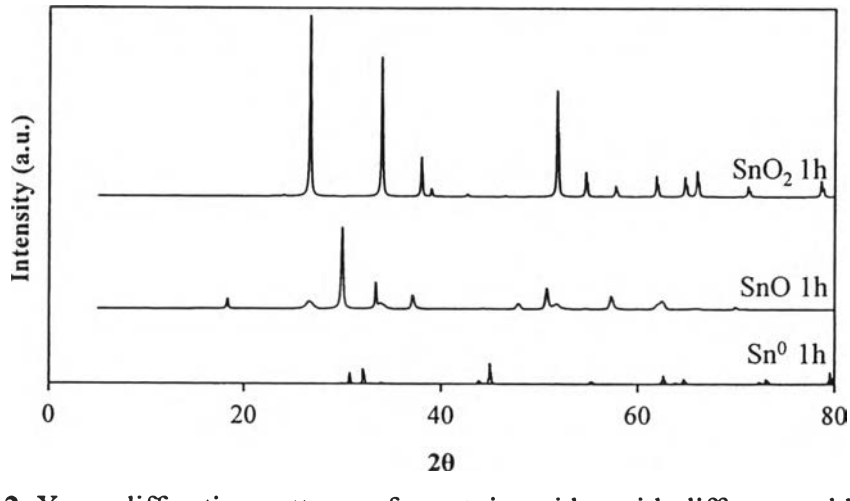

Figure 4.2 X-ray diffraction patterns of spent tin oxides with different oxidation states.

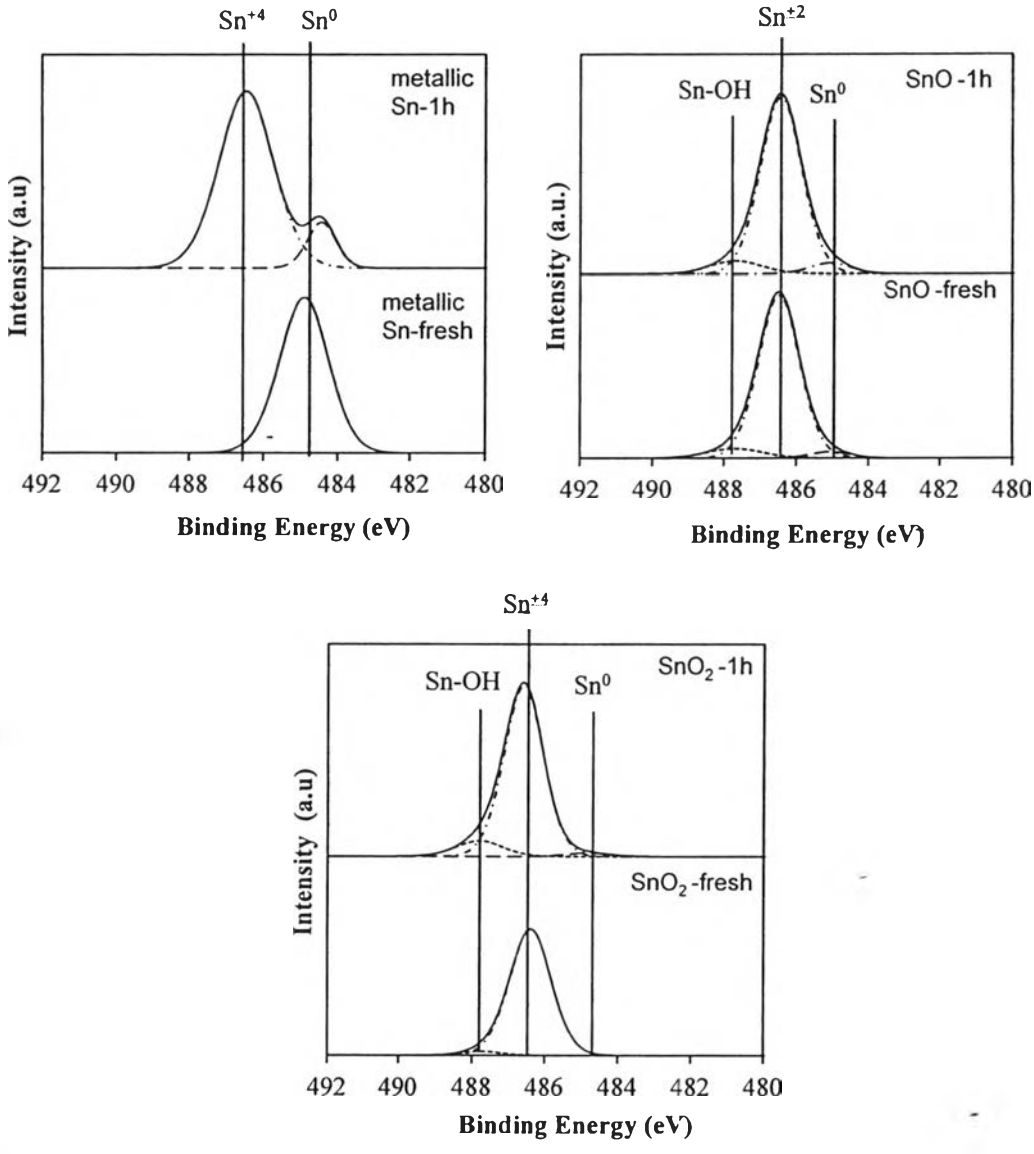

Figure 4.3 Sn $3d_{5/2}$ XPS spectra of (A) fresh and spent metallic tins, and (B) SnO and (C) SnO_2.

The composition of tin species is shown in Table B1 Appendix B. The XPS analysis of fresh and spent catalysts was performed in order to observe the change of binding energy (BE) or oxidation state. After the binding energy calibration, the convolution of the Sn $3d_{5/2}$ was accomplished based on the BE of metallic Sn (485 eV), SnO (486.4 eV), SnO_2 (486.7 eV) (Hwang *et al.*, 2012) and Sn-OH (488) (Krishnakumar *et al.*, 2009). Figure 4.3 shows the fitted curve of metallic tin (A), SnO (B) and SnO_2 (C) before and after the dehydration of bio-

ethanol. The peak of fresh metallic tin located at 485.0 eV is assigned to the oxidation state of 0. The peak of SnO (Sn^{+2}) in Figure 4.3(B) is located at 486.4 eV, while the peaks at BE of 485 and 488 eV are assigned to metallic tin and Sn-OH, accounted for 3.5% and 7.7% on the fresh surface, respectively. The peak of SnO_2 (Sn^{+4}) is at the BE of 486.68 eV, which is account for 88.6%. It is also found from the XPS result that the oxidation state of tin oxides does not significantly change after 1 h of time-on-stream, indicating that the activity testing result are truly contributed from pure SnO and SnO_2. After the reaction testing, for the spent SnO, the percent composition of metallic Sn increases from 3.5% to 5.1%, and Sn-OH group increases from 7.7% to 8.9%. Likewise, for SnO_2 in Figure 4.3(C), the percent composition of Sn-OH group increases from 3.2% to 9.4%. A tin oxide containing –OH group was reported to be naturally hygroscopic (Krishnakumar *et al.*, 2009), which may be able to act as bronsted acid, helping to form bigger hydrocarbons. However, the amount of Sn-OH on spent catalysts slightly increases. This may be because ethanol could adsorb on oxygen vacancy forming ethoxy group, and leaving oxygen-hydrogen atom on the surface (Farfan-Arribas and Madix, 2002). On the other hand, the oxidation state of metallic tin changed to which could be assigned to the oxidation states of 0 and +4 with the relative peak area of 12.5 and 87.5%, respectively. It is well known that tin tends to be oxidized when exposed to an oxidizing atmosphere. This indicates that metallic tin could be oxidized during dehydration reaction.

4.1.1.2 Catalytic Activity of Tin Oxides

The dehydration of bio-ethanol over tin oxides was studied at the temperature of 400 °C. It was found that the conversion of bio-ethanol did not change significantly with or without tin oxides, indicating that bio-ethanol is able to convert to ethylene easily at 400 °C. The yield of extracted oils using all metal oxide with all different oxidation state remains about 0.71% as shown in Appendix A. Figure 4.4 displays the gas distribution obtained from using metallic tin, and tin oxides in the dehydration of bio-ethanol. All catalysts show the decrease in ethylene selectivity and the increase of propylene, cooking gas and butylenes, compared to the non-catalyst case. The selectivity of propylene when SnO was employed is slightly higher than in the metallic Sn and SnO_2 cases. On the other hand, the selectivity of cooking

gas is highest with using metallic Sn. This indicates that metallic tin has hydrogenation property. Since the pore diameters of both SnO and SnO_2 are very large, compared to the kinetic diameters of propylene, cooking gas, and butylenes, the selectivity of small olefins and paraffins is governed by both acid property and pore constraint.

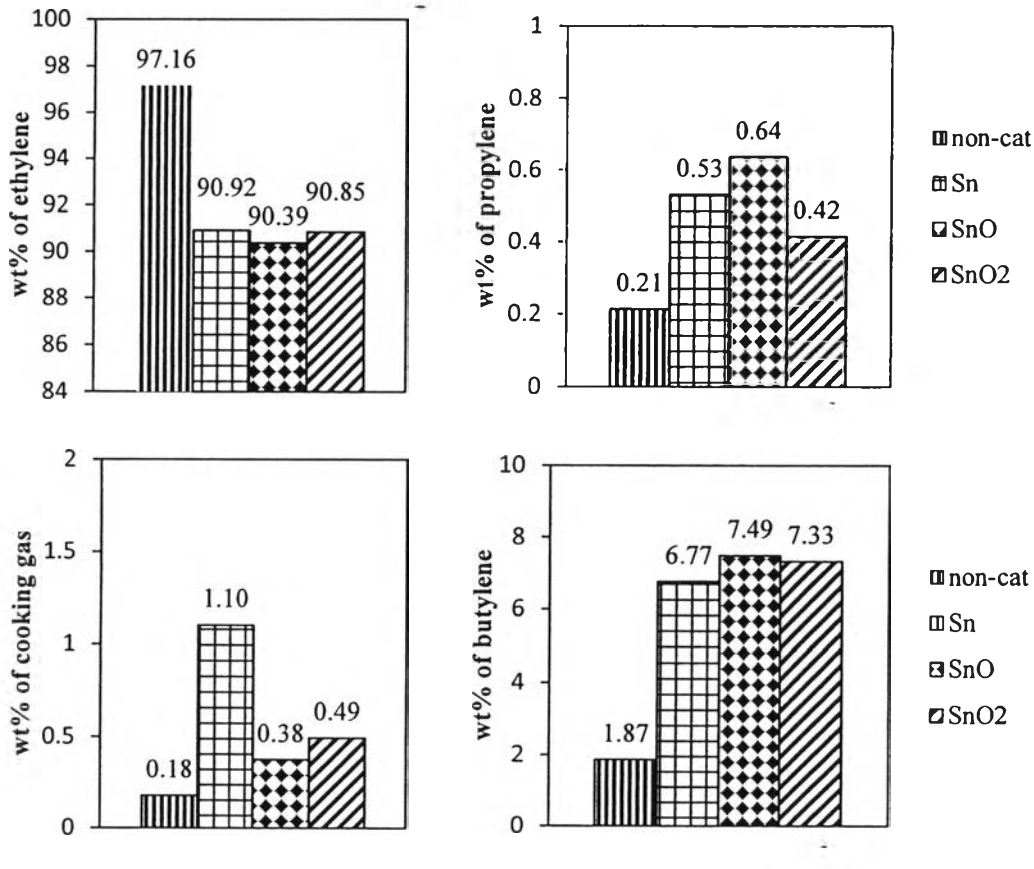

Figure 4.4 Weight percentage of ethylene, propylene, cooking gas and butylenes in gas phase from using metallic tin, SnO, and SnO_2.

The main products in oils using either metallic tin or tin oxide are oxygenates, non-aromatics, and benzene. Even though the oil yield is quite low because of the short time on stream, the oil compositions obtained from metallic Sn, SnO and SnO_2 shown in Figure 4.5 are remarkably different. The selectivity of oxygenates using SnO is promoted significantly, while the selectivity of hydrocarbons seem to be enhanced with using metallic Sn and SnO_2. Without a catalyst, only pentanone and 1,1-diethoxyethane consist in the oil phase, whereas the

majority of oxygenate compounds obtained from all catalysts are propanal, 2-petanone with branches, and ethyl acetate. Methyl-cyclopentane and methyl-cyclopentane are the majority of non-aromatics obtained from using SnO. In the non-aromatics obtained from metallic tin, hexane, and cyclohexane are the main components. The non-aromatics from SnO_2 are mainly consisted of hexane and cyclohexane with and without branches. Because of no pore constraint, ethylene might undergo oligomerization and hydrogenation to form hexane, and cyclization and aromatization to form cyclohexane and benzene, respectively. It is noticed that metallic tin gives more hexane than SnO_2, indicating that metallic tin favors hydrogenation rather than cyclization. According to tin oxides with different oxidation states, It was reported that a tin oxide could produce both oxidation and dehydration products (McCabe and Mltchell, 1984). According to the acid property of a metal oxide, acid strength increases with the number of oxygen substitution on the central atom. Therefore, SnO_2, which has higher acid strength, can promote the formation of aromatics. This infers that SnO_2 can enhance the oligomerization, cyclization, and dehydrogenation reactions more than SnO can do.

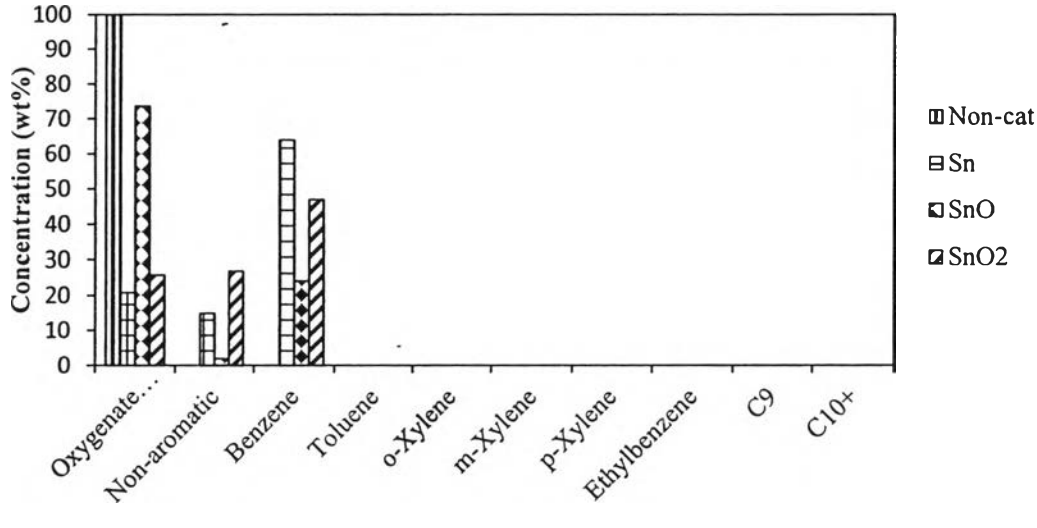

Figure 4.5 Composition of oils using metallic tin, SnO, and SnO_2, compared to the non-catalytic case.

From the result, it can be concluded that metallic is responsible for cooking gas, whereas SnO governed the propylene and oxygenates production. When the oxidation state of tin increase, SnO_2 (Sn^{+4}) is in charge of butylenes and benzene formation.

4.1.2 Interaction between Sn^0 and SAPO-34

In this section, the metallic tin-doped on SAPO-34 was tested in order to examine the effect of an interaction between the metal and support. After metallic tin and SAPO-34 were mixed, followed by H_2 treatment at 400 ˚C for 2 hr, the XPS study was used to determine its interaction. The XPS spectra shown in Figure 4.6 display the change of oxidation state of metallic tin doped on SAPO-34 before and after treatment under hydrogen atmosphere.

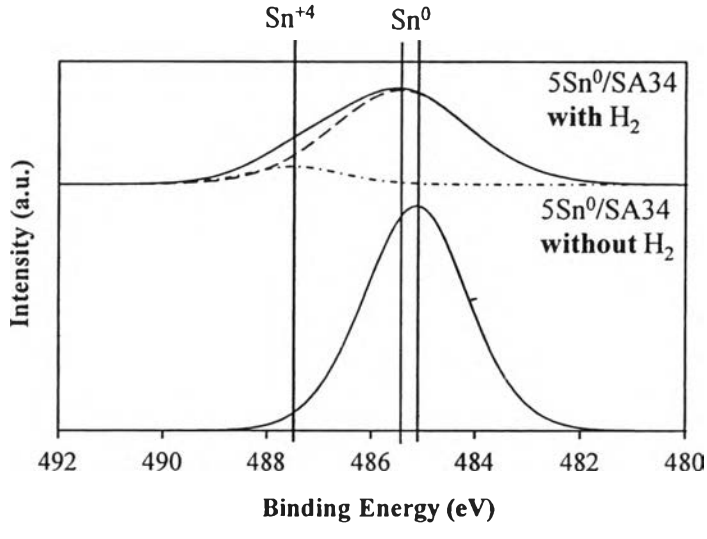

Figure 4.6 Sn $3d_{5/2}$ XPS spectra of $5Sn^0$/SAPO-34 before and after treatment.

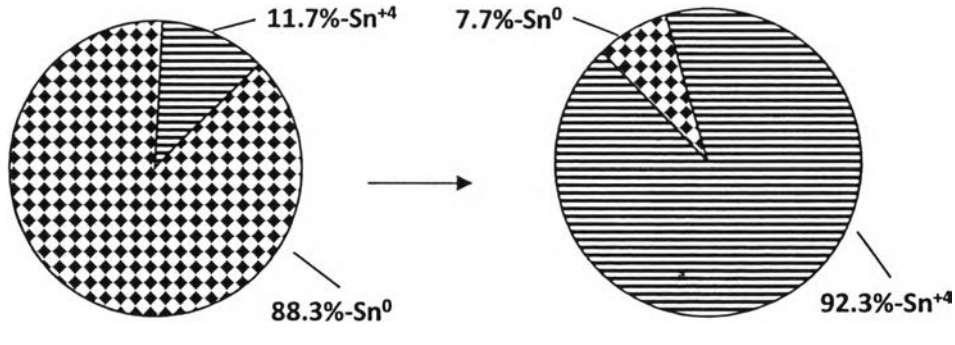

Figure 4.7 Tin species of $5Sn^0$/SAPO-34 before and after reaction.

After H_2 treatment, the peak assigned for metallic tin (485 eV) shifts to about 0.2 eV higher binding energy, indicating that there is an interaction between metallic tin and SAPO-34 support. Some Sn^0 is found oxidized by the SAPO-34 support to form Sn^{+4}, and then the surface composition changes to 88.3% of Sn^0 and 11.7% of Sn^{+4}. After the reaction testing, the percent composition of SnO_2 whose the peak is located at 487.4 eV increases to 92.3% as shown in Figure 4.7. This may be because ethanol could adsorb on oxygen vacancy forming ethoxy group, and leaving oxygen-hydrogen atom on the surface (Farfan-Arribas and Madix, 2002).

Another reason is that Sn^0 may be oxidized during reaction since tin tends to be oxidized when exposed to an oxidizing atmosphere, and water as a by-product of dehydration of bio-ethanol is one of the oxygen sources.

For the catalytic testing, $5Sn^0$/SAPO-34 gives mostly gaseous products. The gas selectivity obtained from $5Sn^0$/SAPO-34 in Figure 4.8 shows the decrease in ethylene selectivity and the increase of propylene, cooking gas and butylenes. It is found that the selectivity of propylene and cooking gas increases significantly, which is similar to the selectivity of cooking gas obtaining from a sole metallic tin shown in Figure 4.4. This indicates that metallic tin is responsible for the high selectivity of cooking gas, and has hydrogenation property. Moreover, the interaction between Sn^0 and the SAPO-34 support with appropriate pore constraint and acidity obviously enhances small paraffin formation.

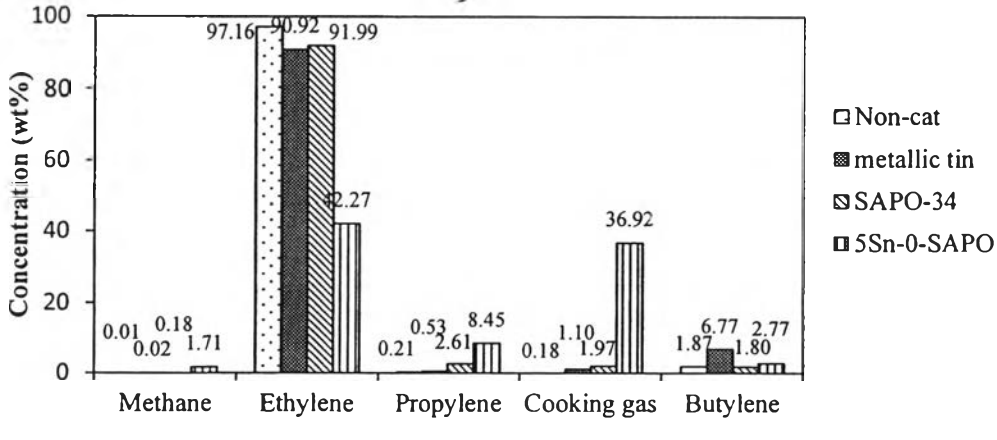

Figure 4.8 Weight percentage of ethylene, propylene, cooking gas and butylenes in gas phase using $5Sn^0$/SAPO-34.

The main products in oils using $5Sn^0$/SAPO-34 displayed in Figure 4.9 consist of only non-aromatics and benzene. In the non-aromatics obtained from $5Sn^0$/SAPO-34, hexane, cyclohexane and ethyl-cyclobutane are the main components, which are all saturated compounds. However, the selectivity of benzene using $5Sn^0$/SAPO-34 is higher than in the metallic tin case. SAPO-34 is considered being one of the acid catalysts. It has both Lewis and Bronsted acid sites where carbenium ion formation from olefin compounds can be promoted. Once cyclization of the formed carbocations has occurred, a proton can be lost or given, and a cyclohexene is obtained. The proton elimination or dehydrogenation reaction could undergo until the benzene is formed. The hydrogen abstracted may be transferred to small olefins, resulting in propane and butane formation as shown in Figure 4.9. Therefore, the dehydrogenation and hydrogenation reactions dominate, and then cooking gas and benzene are obtained the most.

From the result, it can be concluded that support helps the metal oxide to be highly dispersed, and the treatment under the hydrogen atmosphere consequently creates the stronger interaction between metal and support, resulting in higher selectivity of gas that metal is responsible for as the same as that of sole metal.

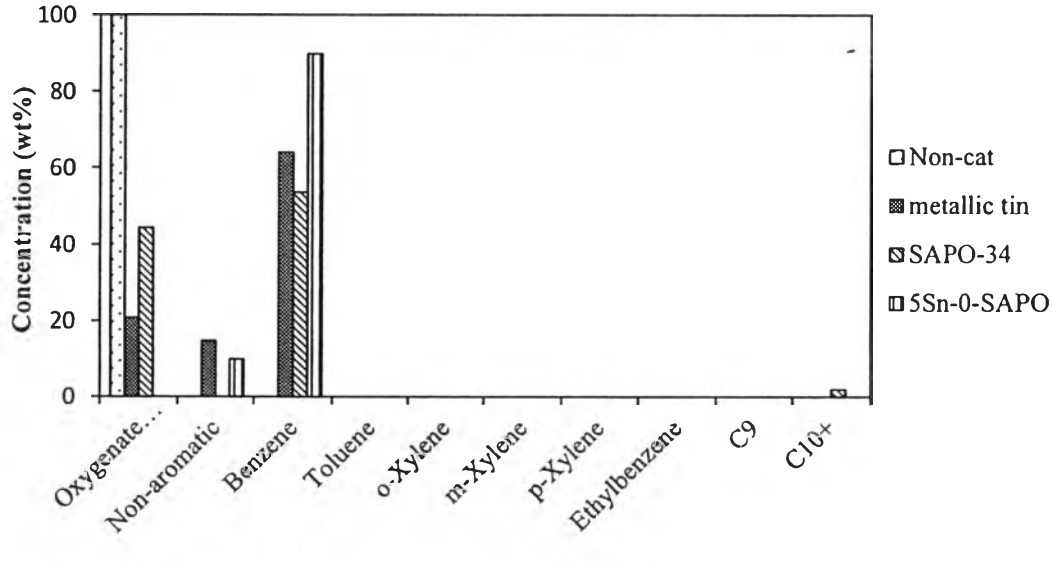

Figure 4.9 Composition of oils using $5Sn^0$/SAPO-34.

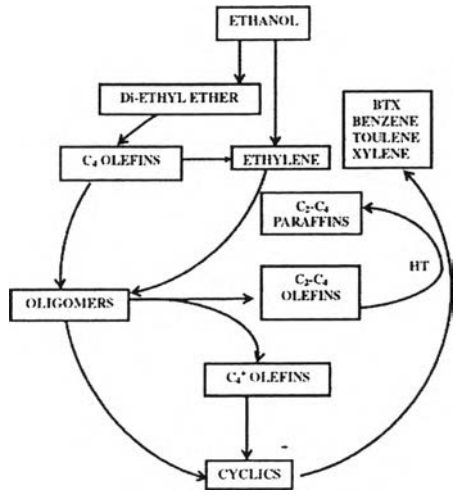

Figure 4.10 Reaction pathway of ethanol to hydrocarbons (Viswanadham *et al.*, 2012).

4.1.3 SnO_x/SAPO-34

The physical properties of modified catalysts were determined based on N_2 physical adsorption using a Thermo Finnigan/Sorptomatic 1990 surface area analyzer. Table 4.4 displays surface areas, pore volume and Horvath Kawazoe (HK) pore diameter of SAPO-34 supported catalysts. The introduction of metal oxides by using solid-solid interaction method leads to the reduction of specific surface area. This is because the metal oxide itself has a much lower surface area than that of the zeolite. Therefore, after doping metal oxides on zeolites via solid-solid interaction method, the average surface area of the catalysts decreases significantly. However, the pore volume increase from 0.22 to 0.26 and 0.29 m^3/g after the addition of 7 wt% of tin and antimony oxides, respectively.

The XPS analysis of fresh and spent catalysts was done in order to observe the changes of oxide phases on SAPO-34 versus time-on-stream through the changes of binding energy (BE). The binding energy was calibrated by using C 1s spectra as the reference located at BE=285 eV for all catalyst samples.

Table 4.3 Specific surface areas and pore characteristics of SAPO-34 supported catalysts

Catalyst	Calcination Temperature (°C)	BET area (m^2/g)	Pore Diameter (Å)	Pore Volume (m^2/g)
SAPO-34	400	364.4	7.6	0.22
5SnSAPO-34	400	315.2	7.1	0.18
7SnSAPO-34	400	296.0	7.0	0.17
5SbSAPO-34	400	268.4	7.2	0.19
7SbSAPO-34	400	258.2	7.1	0.18
5SnSAPO-34	700	247.9	8.3	0.17
7SnSAPO-34	700	249.8	8.8	0.26
5SbSAPO-34	700	267.3	7.9	0.16
7SbSAPO-34	700	236.3	7.2	0.29

After the binding energy calibration, the convolution of the Sn 3d was performed by considering the BEs of metallic Sn (485 eV), SnO (486 eV), SnO_2 (486.7-487 eV) and Sn-OH (488.1-488.5).

For 5wt% of tin oxide on SAPO-34, the changes of species and composition of tin oxide on SAPO-34 are shown in Figure 4.11. All XPS spectra indicate mixed oxide phases at every time-on-stream. At initial, the peaks at 488.3 eV and 487 eV are assigned to Sn–OH and SnO_2, respectively. After the catalytic dehydration of ethanol was carried out, the phase composition of tin oxides on the surface changes as shown in Figure 4.13. Sn^0 starts to form at 180 time-on-streams, decreases after 300 time-on-streams, and then disappears at 480 min time-on-stream. This indicates that the gain and loss of tin oxide phases occurred from the oxidation and reduction reactions. For 7 wt% tin oxide-doped SAPO-34 catalyst, Figure 4.12 represents the fitted curves of Sn $3d_{3/2}$ of fresh and spent catalysts versus time-on-stream. From the fitting results, all curves from XPS are well fitted with Gaussian type distribution, although the XPS spectra of catalysts show a slightly asymmetric peak, indicating mixed valence oxidation states. Figure 4.14 displays the changes of composition of Sn species on the surface of 7wt% SnO_x/SAPO-34. The two different

peaks of fresh catalyst could be assigned to SnO_2 and Sn-OH, which account for 78% and 22%, respectively. At the initial 60 min of reaction time, the XPS peaks show the disappearance of –OH group and the reduction of SnO_2. On the other hand, Sn^0 starts to appear on the surface with 60% atomic composition. However, at 180 and 300 min time-on-streams, the amounts of SnO_2 and metallic tin are regained back and forth. At the end of 480 min, the binding energies of peaks did not fit into any type of tin oxide, suggesting that the support and tin oxide might partially form a mixture. It is noticed that, from the XRD spectra shown in Appendix C Figure C2, there is a new peak located at 2θ=65°.

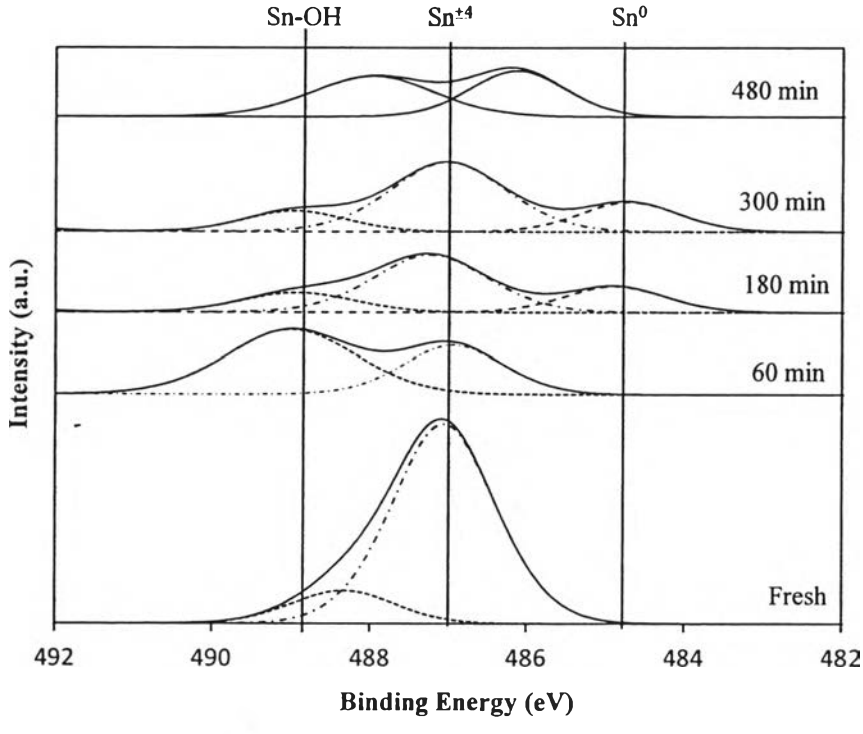

Figure 4.11 XPS spectra of 5SnSAPO-34 calcined at 400 ˚C before and after catalyst performance testing.

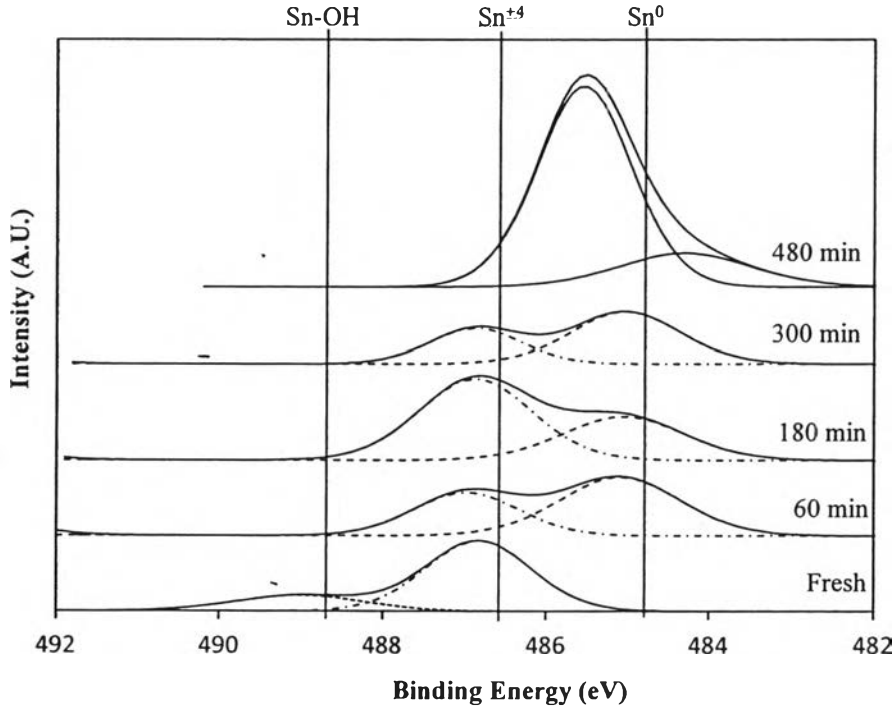

Figure 4.12 XPS spectra of 7SnSAPO-34 calcined at 400 °C before and after catalyst testing.

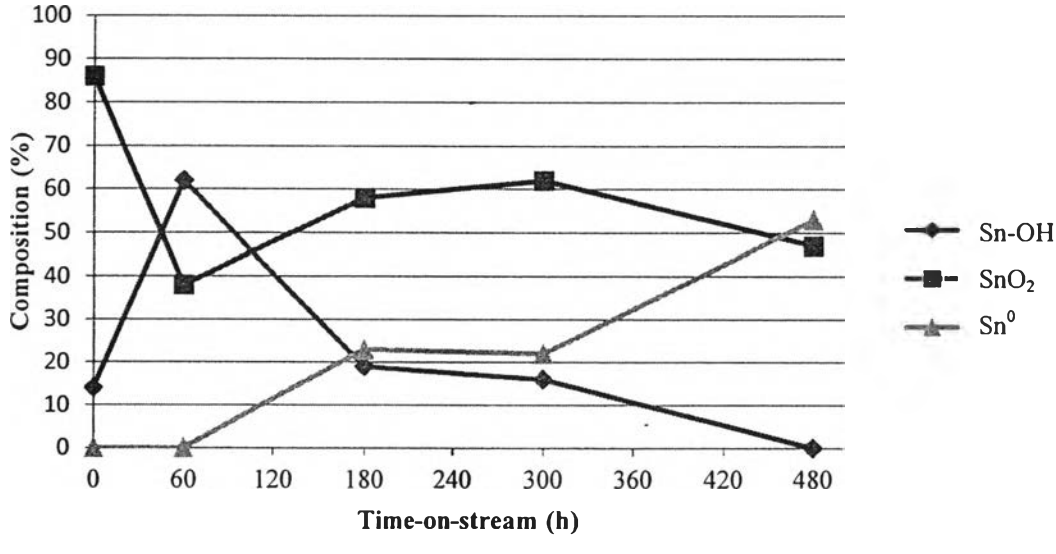

Figure 4.13 Changes of species and compositions of tin oxides on 5 wt% tin oxide-doped SAPO-34 with time-on-stream.

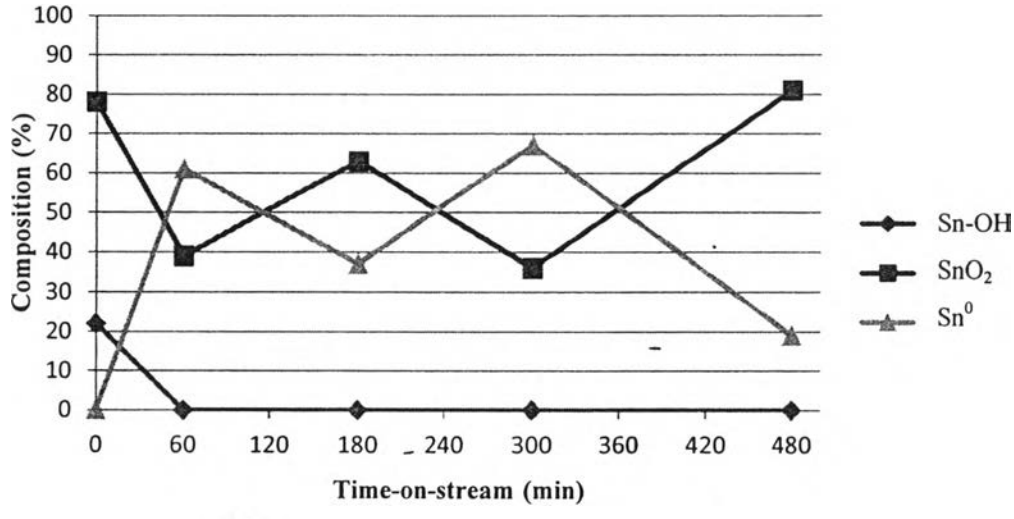

Figure 4.14 Changes of species and compositions of tin oxides on 7 wt% tin oxide-doped SAPO-34 with time-on-stream.

The effects of catalysts on product distribution for the catalytic dehydration of bio-ethanol were studied as a function of time-on-stream. For the catalytic performance of 5 and 7wt% Sn_xO_y/SAPO-34, the bio-ethanol conversion stayed approximately 97.5% throughout the period of 60, 180, 300 and 480 min. However, the catalysts show a significant difference in gas selectivity and liquid composition through the period of reaction time. The gas yield decreases with increasing time-on-stream, whereas the liquid yield increases. It is also observed that, at any time-on stream, the extracted oil yield from 5SnSAPO-34 is slightly lower than that of 7SnSAPO-34, meaning that the increase of metal oxide loading can enhance oil yield. Figure 4.15 shows gaseous product distributions of 60, 180, 300 and 480 min time-on-stream. 5SnSAPO-34 gives 78.2% of ethylene yield, which is much higher than that of 7SnSAPO-34 at the initial 60 min. On the contrary, the yields of propylene and propane increase with increasing the loading percentage of tin oxide. After 60 min of reaction time, ethylene is the main product. The gas selectivity of ethylene, propylene, propane and butane in Figure 4.15 is fluctuated as the amount of SnO_2 species on 5wt% and 7wt% tin oxide-doped SAPO-34 in Figures 4.11 and 4.12 respectively, changes. This indicates that SnO_2 (Sn^{+4}) governs the production of propylene, cooking gas and butylenes.

In addition, the TBP curves of extracted oils obtained from 5 and 7wt% tin oxide-doped SAPO-34 catalysts are cut into petroleum fractions as shown in Figures 4.16 and 4.17. The extracted oils from both of 5SnSAPO-34 and 7SnSAPO-34 fall into the gasoline range of more than 70%. It can be seen that kerosene and gas oil increase simultaneously with increasing time-on-stream, especially at 480 min time-on-stream. This may due to the accumulation of C10+ aromatics.

Initially, the XPS spectra of 7SnSAPO-34 consist of two different peaks, which could be assigned to Sn-OH and SnO_2. The sample containing –OH group is reveals that tin oxide is hygroscopic in nature (Krishnakumar *et al.*, 2009) which may contribute to the ethylene formation as well as tin oxide. According to the dehydration of ethanol reported by Shinohara *et al.* (1998), ethanol could adsorb either on hydroxyl group or metal cation of metal oxide surface, which could undergo further reaction to form ethylene or oxygenate compound. This indicates the formations of propylene and propane are improved when tin oxides with oxidation state +4 or higher was added, resulting from the increase of acidity. At the initial 60 min, the result of XPS analysis shows that the amount of metallic tin increases, indicating the reduction of tin oxide. Jung *et al.* (2000) found that zinc oxide could be reduced by primary alcohol, forming carbon dioxide and water as by-product. However, the obtained gaseous product did not contain carbon dioxide. This implies that tin oxide is not reduced by ethanol. Based on the n-semiconductor property of tin oxide, propylene could adsorb on tin oxide surface, and forming allylic intermediates as reported by Seiyama *et al.* (1972). From the result of extracted oil composition analyzed by GC-TOF, the majority of liquid compounds is benzene. This indicates that propylene is adsorbed on the metal cation via phi-bond. SnO_2, which has moderate strength and optimum nucleophilic oxygen, could abstract proton from the propylene, forming hydroxyl group and carbanion. Subsequently, the electron from carbanion is transferred to the catalyst, resulting in the dimerization of olefins, followed by aromatization, to benzene. Water is produced from the combination of proton and hydroxyl group, which leads to the reduction of tin oxide and the increase of metallic tin and oxygen vacancy on the surface. Therefore, the reduction of tin oxide may occur through aromatization of benzene. From the peaks at 60, 180 and

300 min of reaction time, the amounts of tin oxide and metallic tin are fluctuated, indicating that the oxygen atoms leave and refill the vacancies sites.

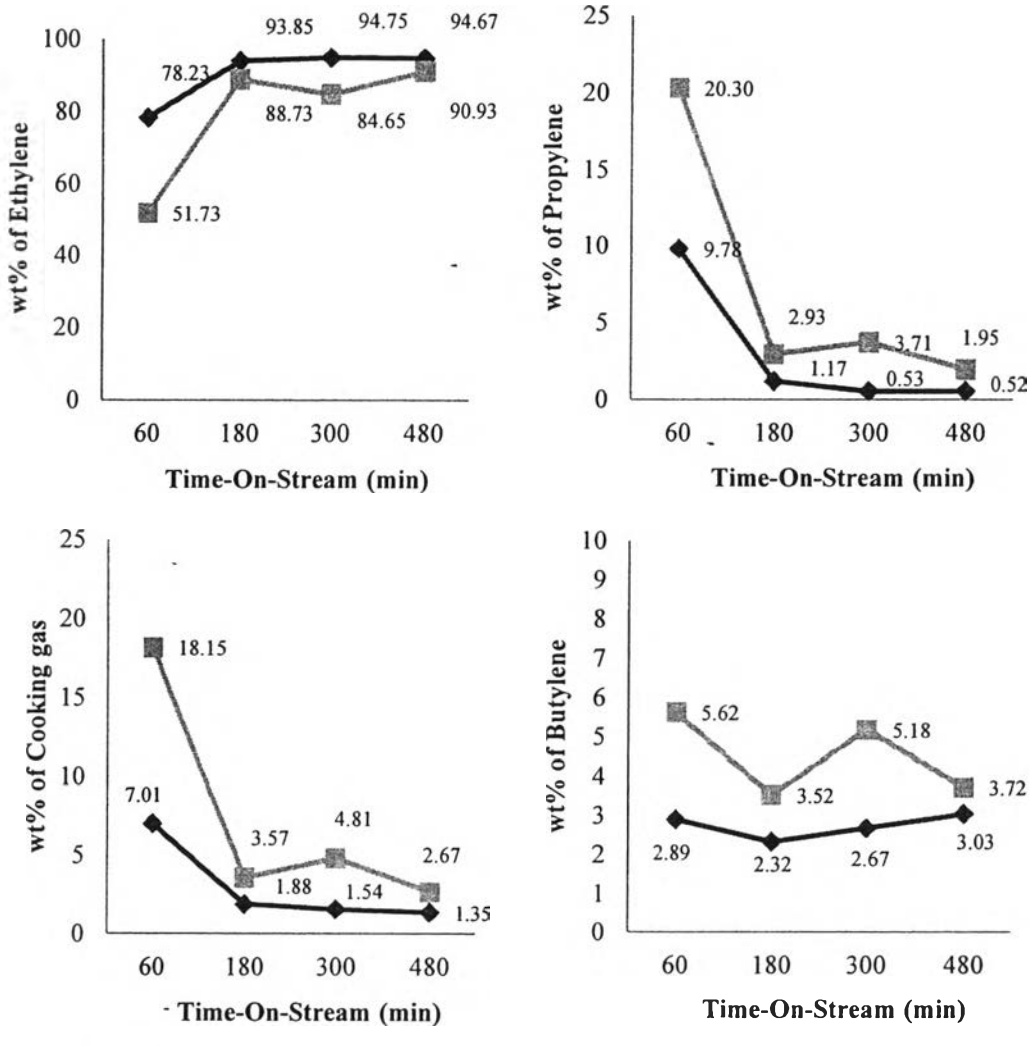

Figure 4.15 Weight percentage of ethylene, propylene, cooking gas and butylene in gas phase from using 5wt% (♦) and 7wt% (■) of tin oxide on SAPO-34.

$$CH_3CH_2O_{(a)} \rightarrow CH_2{=}CH_{2(g)} + H_{(a)} + O_{(l)}$$

Scheme 4.1 Formation of ethylene from adsorbed ethoxide species (Farfan-Arribas and Madix, 2002).

Farfan-Arribas and Madix (2002) had reported that ethanol could adsorb on oxygen vacancy, forming ethoxy group. The ethylene is formed by leaving the oxygen atom on the surface as shown in Scheme 4.1. In addition, the oxygenate compounds from 5wt% SnO_x/SAPO-34 are mainly 2-pentaone, Cyclopentanone, hexanone, 2-methyl and 13-Tetradecynoic acid, methyl ester while the majority of oxygenate product from 7wt % of tin oxide are 2-pentanone and large molecule of ester.

Therefore, SnO_2 (Sn^{+4}) on SAPO-34 governs the formation of propylene, cooking gas butylenes and benzene, which the unsupported SnO_2 behaves similarly, which gives the same composition of gas and oil. However, due to the interaction between the metal oxide and support, the heavy hydrocarbons, like C10+ aromatics and large molecule of oxygenates, can be formed. The product distribution of 5 wt% SnO_x/SAPO-34 is similar to that of 7wt% SnO_x/SAPO-34.

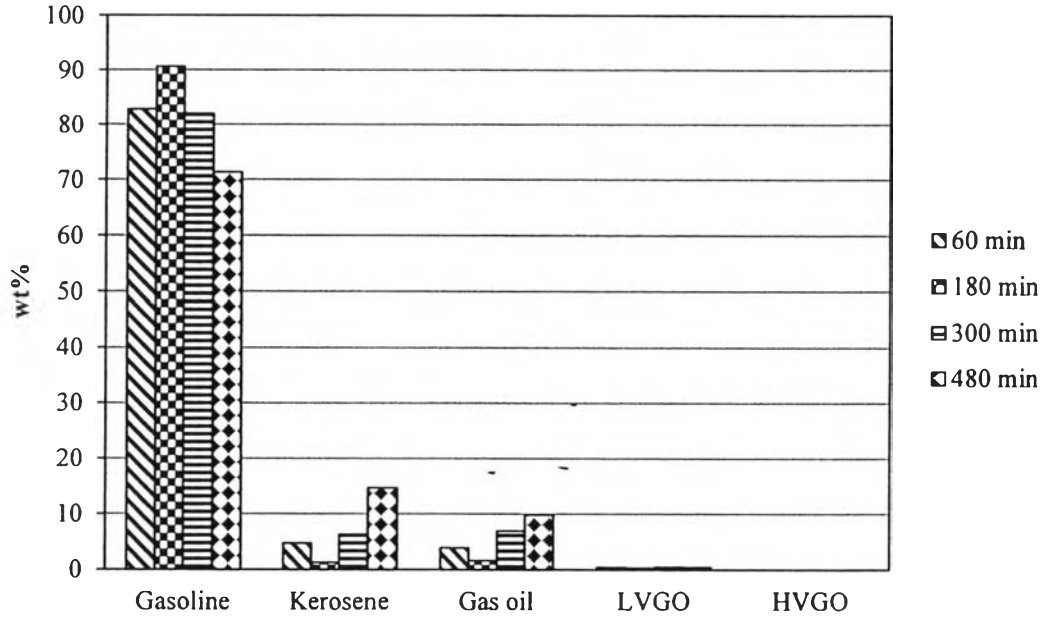

Figure 4.16 Petroleum fractions in oils from 5wt% SnO_x/SAPO34.

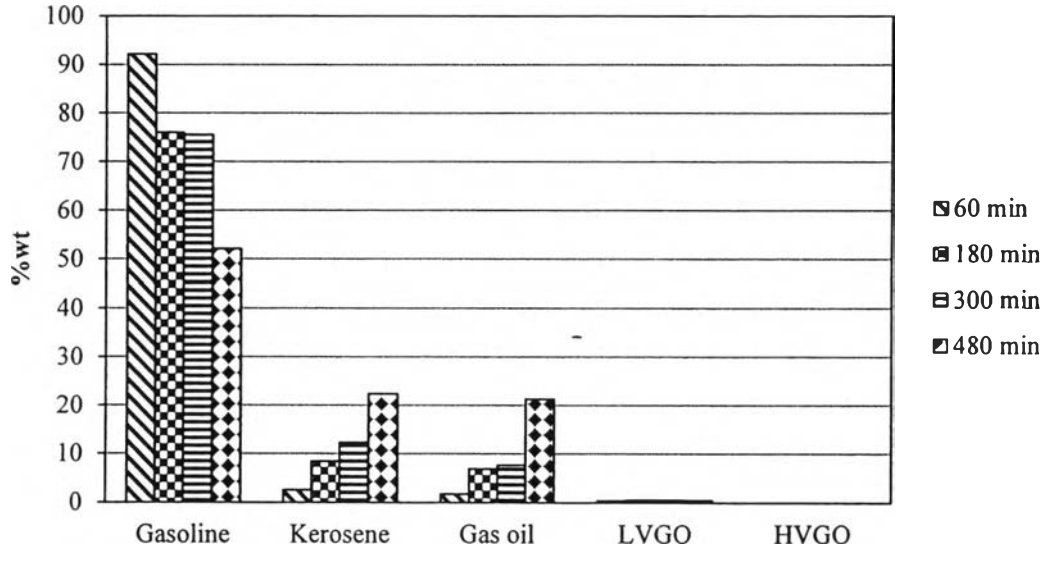

Figure 4.17 Petroleum fractions in oils from using 7wt% SnO_x/SAPO34.

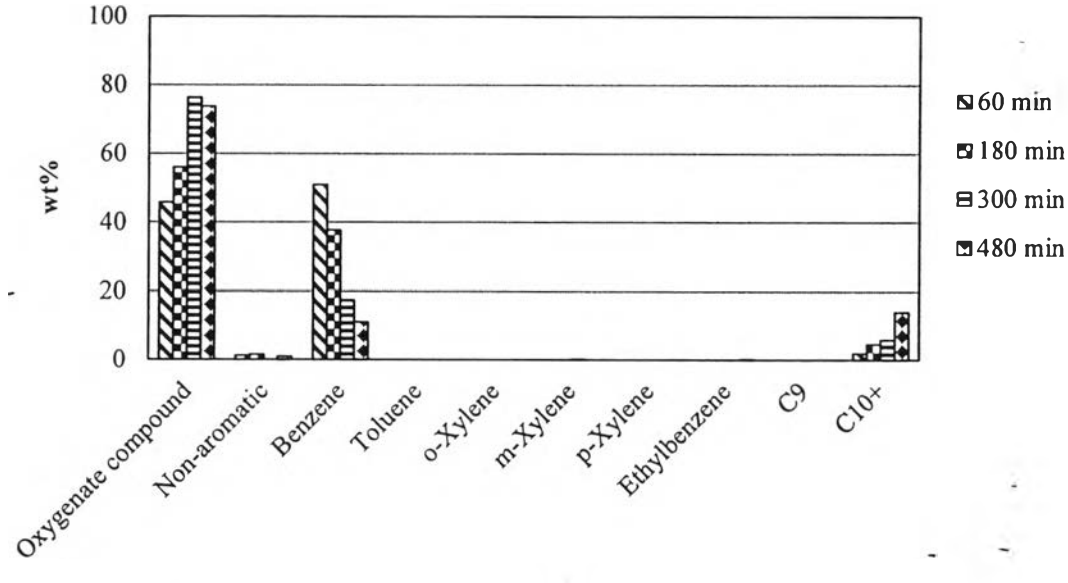

Figure 4.18 Composition of extracted oils from using 5wt. % SnO_x/SAPO-34.

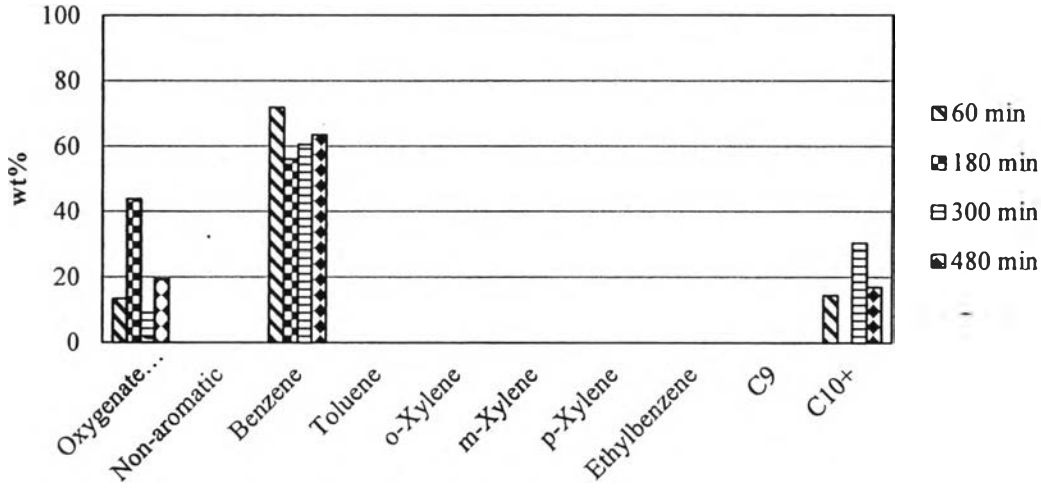

Figure 4.19 Composition of extracted oils from 7 wt. % SnO_x/SAPO-34.

In this section, the effect of calcinations temperature was observed in order to see the change of product distribution in the catalytic dehydration of bio-ethanol. The tin oxide species present on SAPO-34 catalysts when calcined at 400 C° and 700C° were evaluated by using XPS displayed in Figures 4.21 and 4.22. After, curve fitting procedure, the XPS spectrum of fresh catalyst indicates a shift of the Sn $3d_{5/2}$ binding energy toward lower values as the calcination temperature increases to 700C°. The peak positions are assigned to Sn-OH and SnO, instead of Sn-OH and SnO_2. This suggests a weak interaction between tin oxide and catalyst. After the reaction testing, the peak positions are ascribed to Sn^0 and Sn^{+4} species, indicating tin oxide might convert itself from metastable form (Sn^{+2}) to more stable form (Sn^0 and Sn^{+4}).

As can be seen from Figure 4.23, using 5wt. % tin oxide-dope SAPO-34 catalysts and calcined at 400 C°, the yield of propylene and cooking gas was higher than those obtained modified SAPO-34 calcined at 700 C° shown in Figure 4.23. This may be caused from the initial different oxidation state of tin oxide. From reaction pathway purposed by Viswanadham *et al.* (2012), the formation of butylenes required less acid strength than the formation of propylene and small molecule of paraffins. Therefore, the yield of propylene and cooking gas can be enhanced when Sn^{+4} species is presented. On the other hand, the Sn^{+2} species which

have less acid strength than Sn^{+4} species could help to form butylenes. After 60 min time-on-stream, the yield of propylene decreases significantly, indicating that propylene might be converted to other bigger hydrocarbons.

From the TBPs curves of the extracted oil using 5 wt. % of tin oxide-doped SAPO-34 catalyst, the oil from the one with calcinations temperature of 400 C° highly consists of gasoline and almost 20% of kerosene, while the obtained oil from the modified SAPO-34 calcined at the temperature of 700 C° fall into gasoline solely, shown in Figure 4.24. This may due to the higher amount of remaining Sn^{+4}, which have higher acid strength than Sn^{+2} and Sn^{0}, before and after reaction of 5 wt. % tin oxide-doped SAPO-34 with calcinations temperature of 400 C°, can help the formation of big hydrocarbons. From Figures 4.25 and 4.26, the obtained oils from both catalysts highly consist of oxygenate compounds, benzene, and C+10 aromatics with different percent yield versus time.

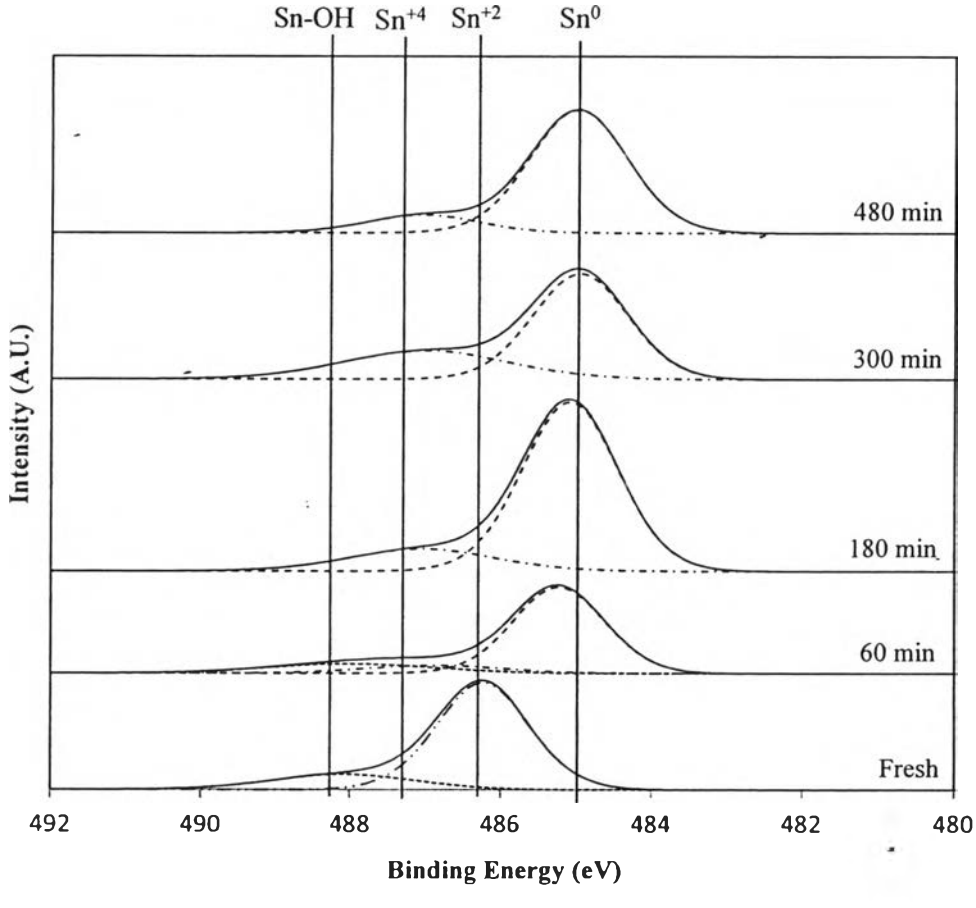

Figure 4.20 XPS spectra of fresh and spent 5SnSAPO34 calcined at 700 °C.

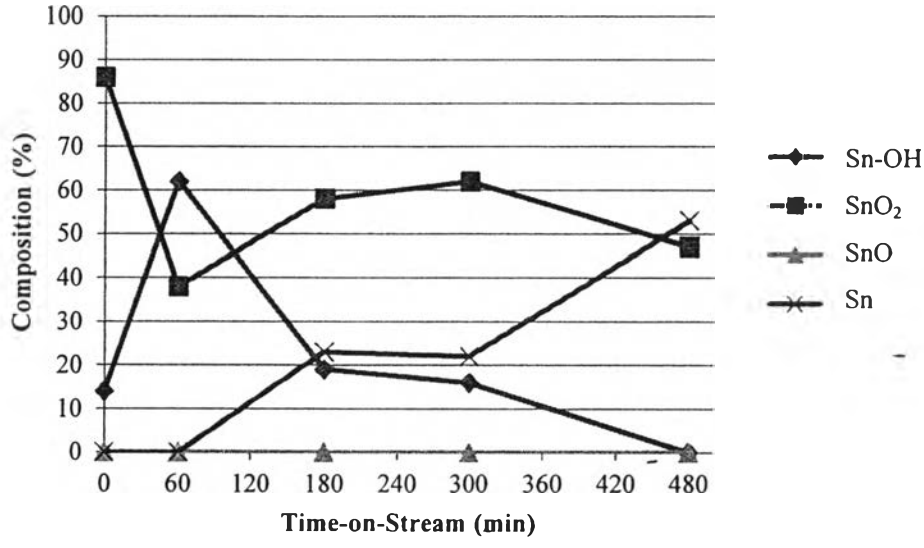

Figure 4.21 Changes of species and compositions of tin oxides on 5 wt.% tin oxide-doped SAPO-34 calcined at 400 °C with time-on-stream.

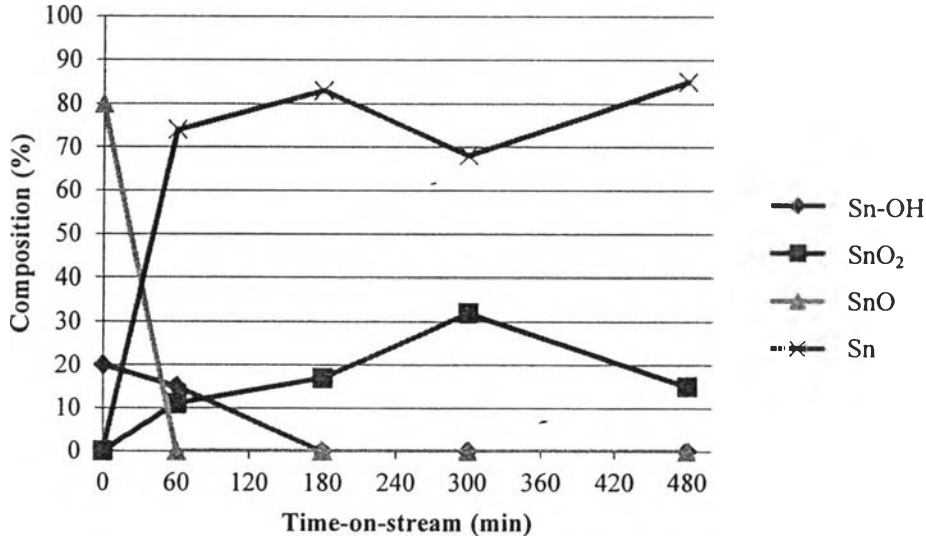

Figure 4.22 Changes of species and compositions of tin oxides on 5 wt.% tin oxide-doped SAPO-34 calcined at 700 °C with time-on-stream.

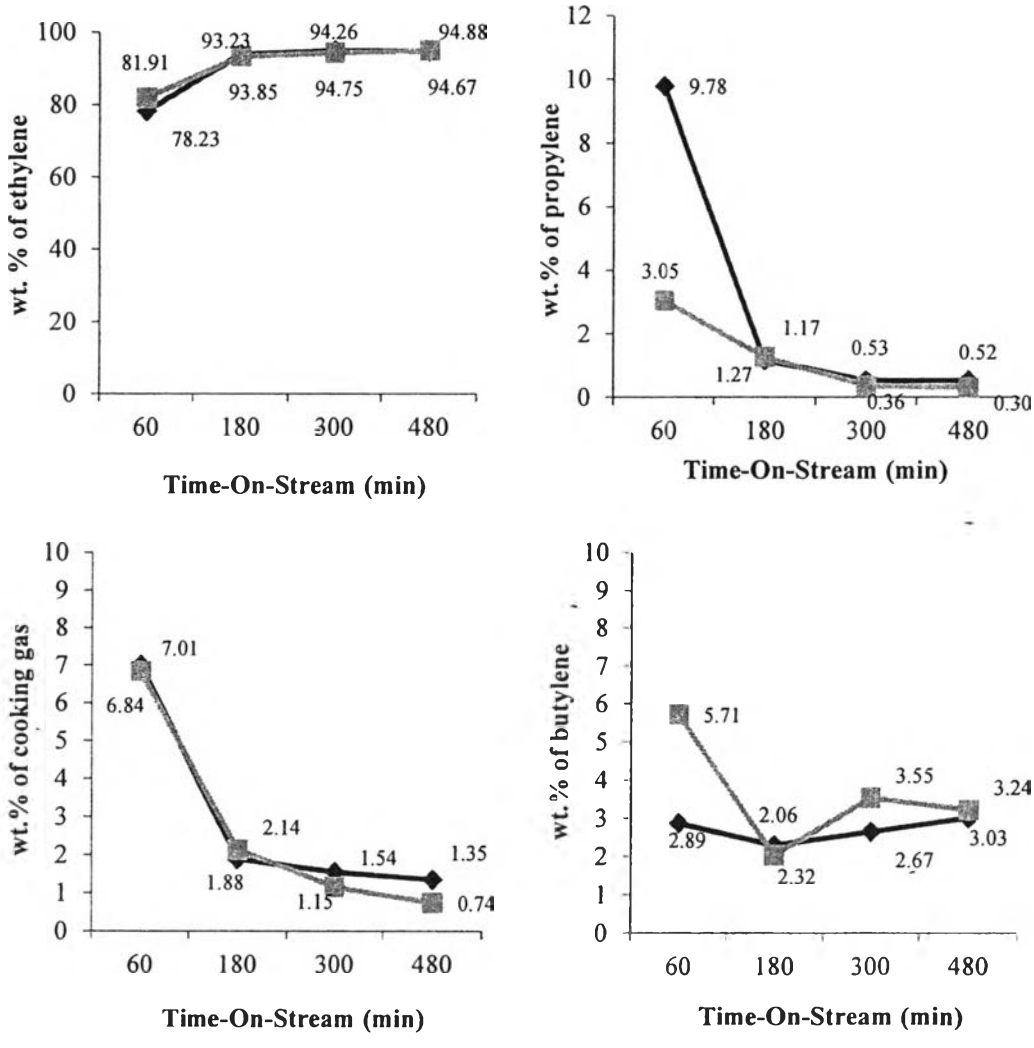

Figure 4.23 Weight percent of ethylene, propylene, cooking gas and butylenes from using 5 wt. % of tin oxide on SAPO-34 calcined at 400 C°(♦) and 700C°(■), respectively.

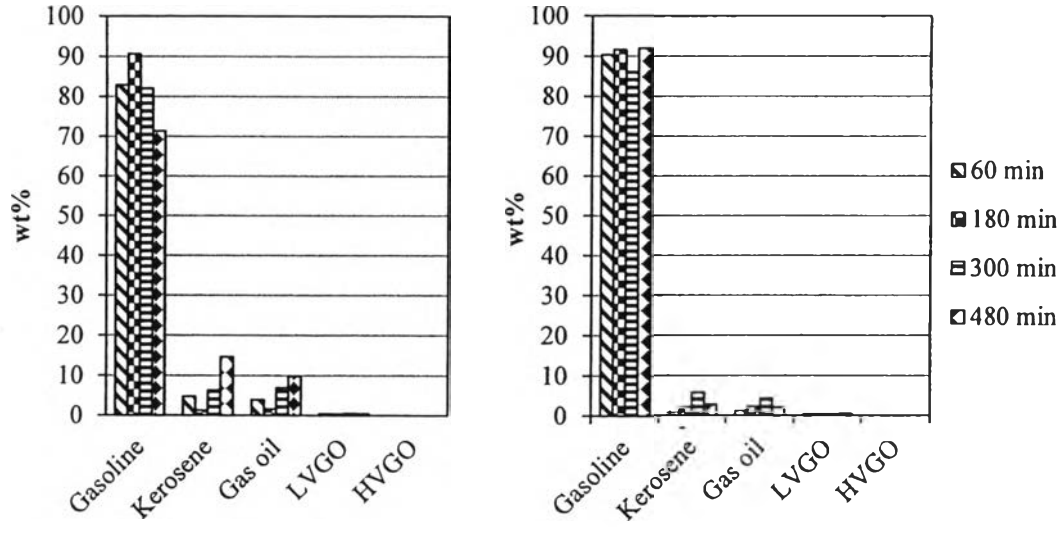

Figure 4.24 Petroleum fractions in oils from using 5 wt. % of tin oxide doped SAPO-34 catalyst calcined at 400 C° (left) and 700 C°(right).

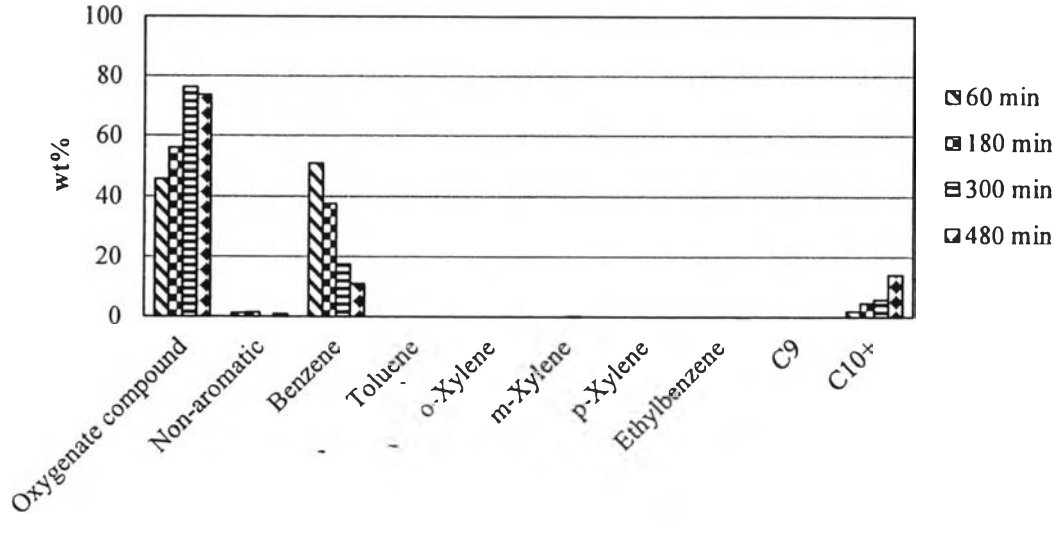

Figure 4.25 Composition of extracted oils from 5 wt.% of tin oxide-doped SAPO34 catalyst calcined at 400 °C.

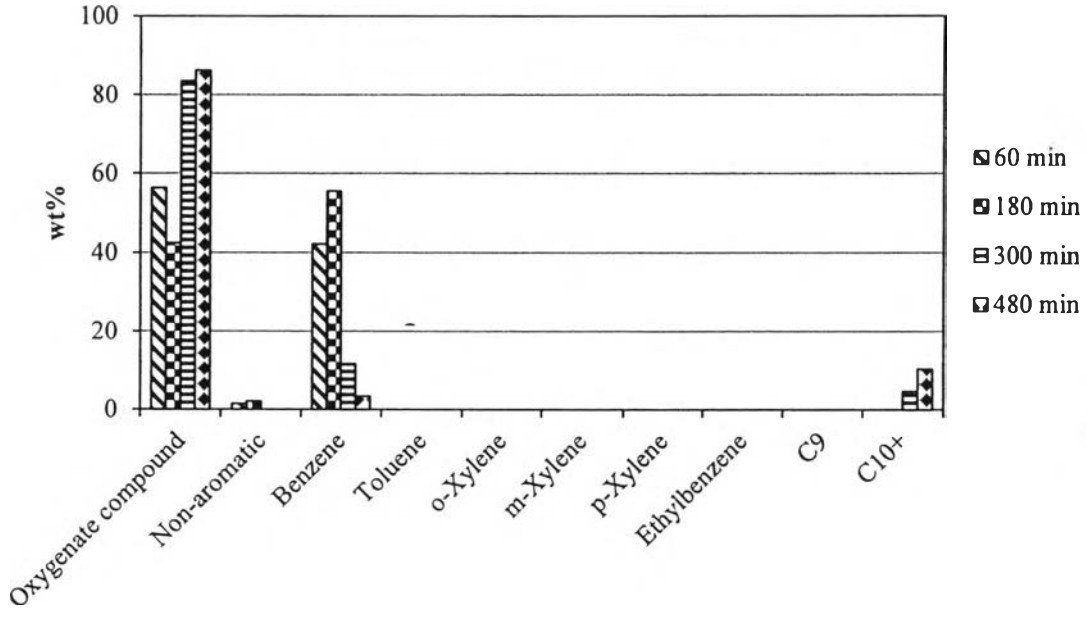

Figure 4.26 Composition of extracted oils from 5 wt.% of tin oxide-doped SAPO34 catalyst calcined at 700 °C.

The oxygenate compounds from using 5wt% SnO_x/SAPO-34 calcined at 400 °C are mainly 2-pentaone, cyclopentanone, hexanone, 2-methyl and 13-Tetradecynoic acid, methyl ester while the majority of oxygenate products from 5wt % of tin oxide calcined at 700 °C is 2-pentanone.

Furthermore, The Sn $3d_{5/2}$ spectra for the fresh and spent 7 wt. % of tin oxide SAPO-34 catalysts with difference of calcinations temperature are compared in Figures 4.28 and 4.29. The XPS spectra indicate a shift of the Sn 3d5/2 binding energy of 7 wt. % of tin oxide doped SAPO-34 toward lower values as the calcinations temperature increased to 700C°, which are also ascribed to Sn^{+2} and Sn-OH. This indicates that the calcinations temperature has influence on the oxidation state of tin oxide. After the reaction was carried out versus time-on-stream, the percent concentration of oxidized tin species changed during the period of reaction time. At 60 min time-on-stream, the oxidation state of tin oxide on SAPO-34 catalysts calcined 400 C° was reoxidized and reduced through the reaction time while that of modified SAPO-34 calcined at 700 C° stayed constant. The gaseous product distribution from using 7 wt. % of tin oxide-doped SAPO-34 catalysts with

calcinations temperature of 400 C° and 700 C° are compared in Figure 4.30. The gas yield of propylene, cooking gas and butylenes from using 7 wt. % of tin oxide doped SAPO-34 at calcination temperature of 400 C° is much higher than that of the modified SAPO-34 catalyst with calcinations temperature of 700 C°, especially the yield of propylene. This may be caused by the different oxidation state of tin oxide on both catalysts. Moreover, at any time-on-stream, the catalyst with the calcinations temperature of 400 C° shows a higher percent yield of ethylene, propylene, cooking gas and butylenes. It can be noticed that the catalyst with the higher existing percent concentration of Sn^{+4} before and after any time-on-stream gave higher gas yield due to higher acid strength. Additionally, as can be seen in Figure 4.31, the derived oils from both catalysts highly consist of gasoline. However, the obtained oil from using 7 wt. % of tin oxide doped on SAPO-34 catalyst with calcinations temperature of 400 C° also consists of kerosene and gas oil up to 23 wt.% and 21 wt.%, respectively with increasing time-on-stream.

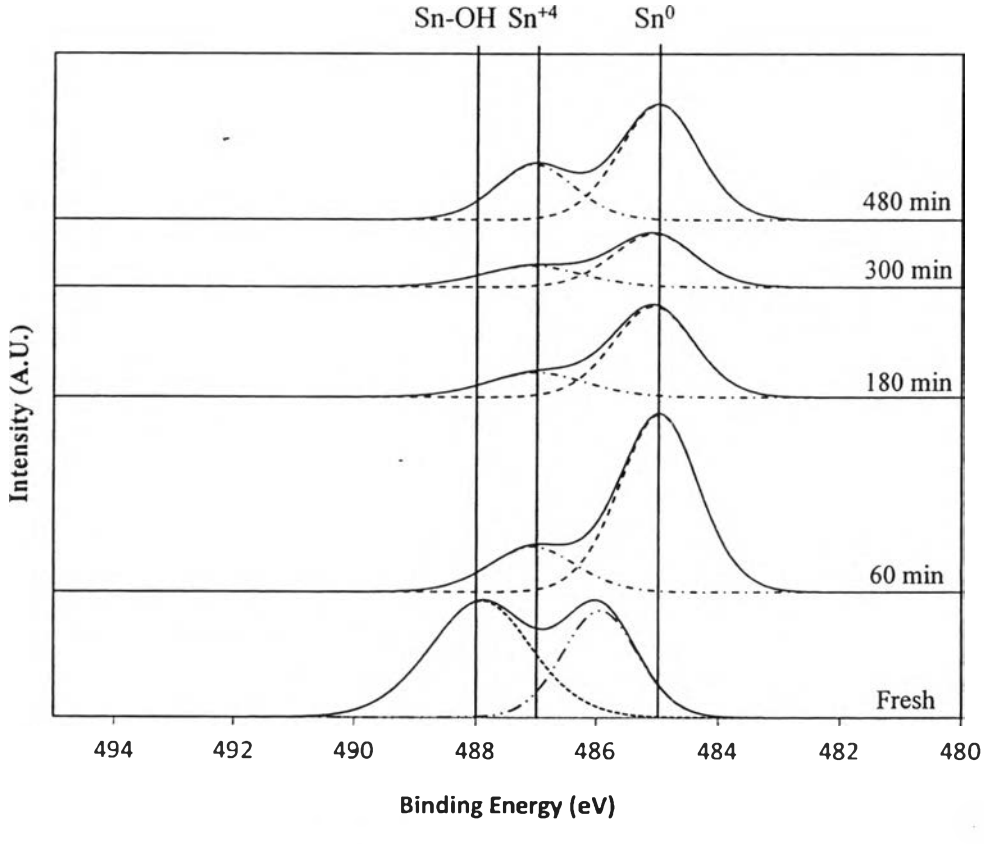

Figure 4.27 XPS spectra of fresh and spent 7SnSAPO34 calcined at 700 °C.

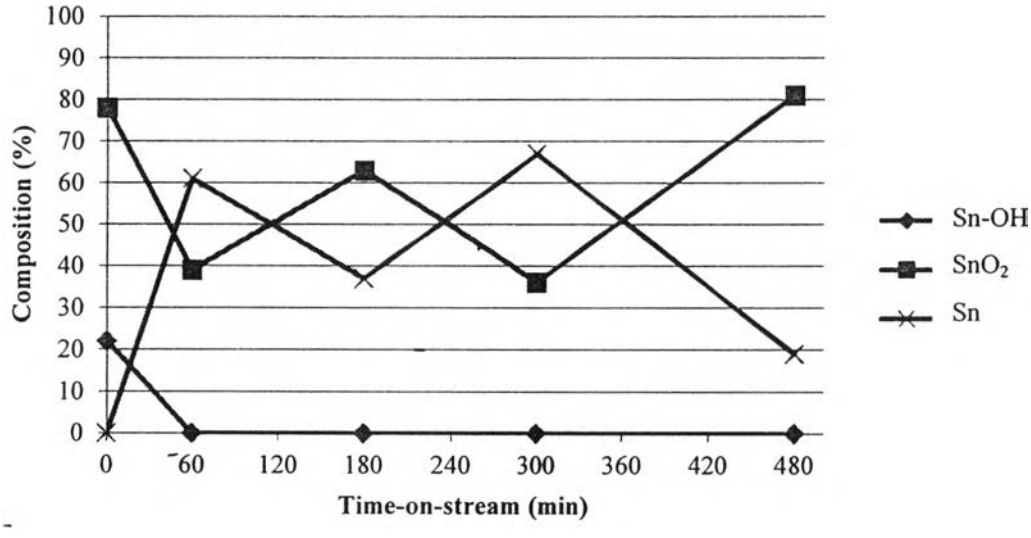

Figure 4.28 Changes of Species and compositions of tin oxides on 7 wt.% tin oxide-doped SAPO-34 calcined at 400 °C.

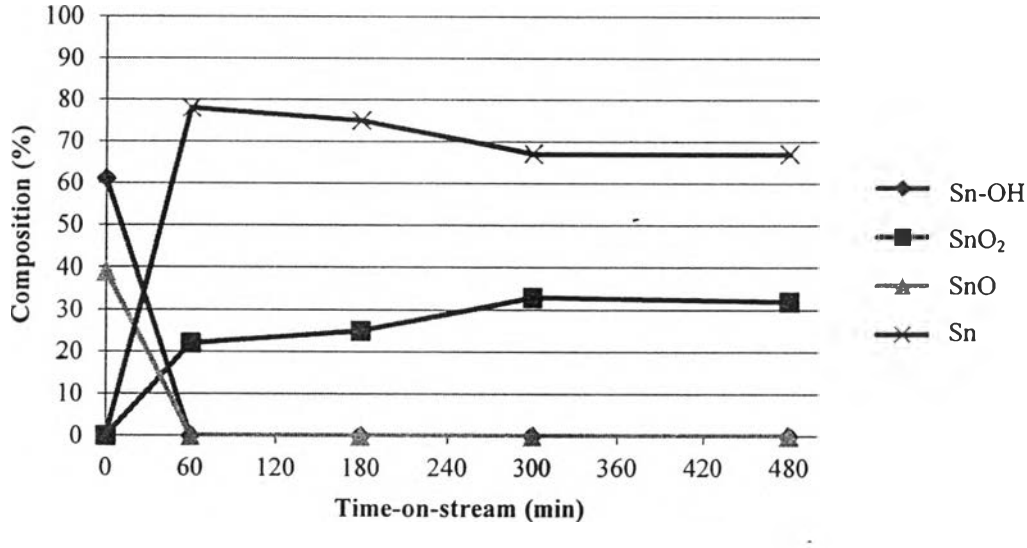

Figure 4.29 Changes of Species and compositions of tin oxides on 7 wt.% tin oxide-doped SAPO-34 calcined at 700 °C.

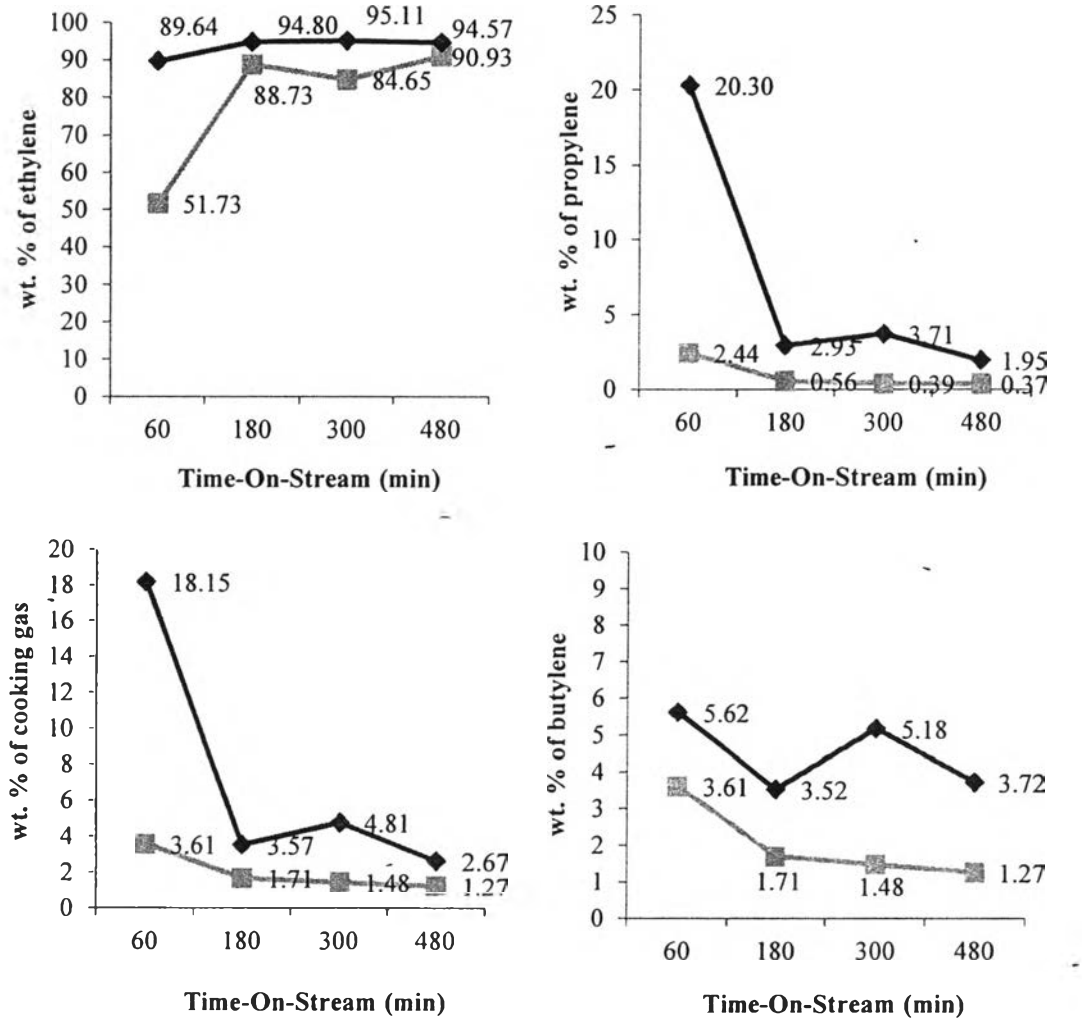

Figure 4.30 Percent weight of ethylene, propylene, cooking gas and butylenes from using 7 wt. % of tin oxide on SAPO-34 calcined at 400 C°(♦) and 700C°(■), respectively.

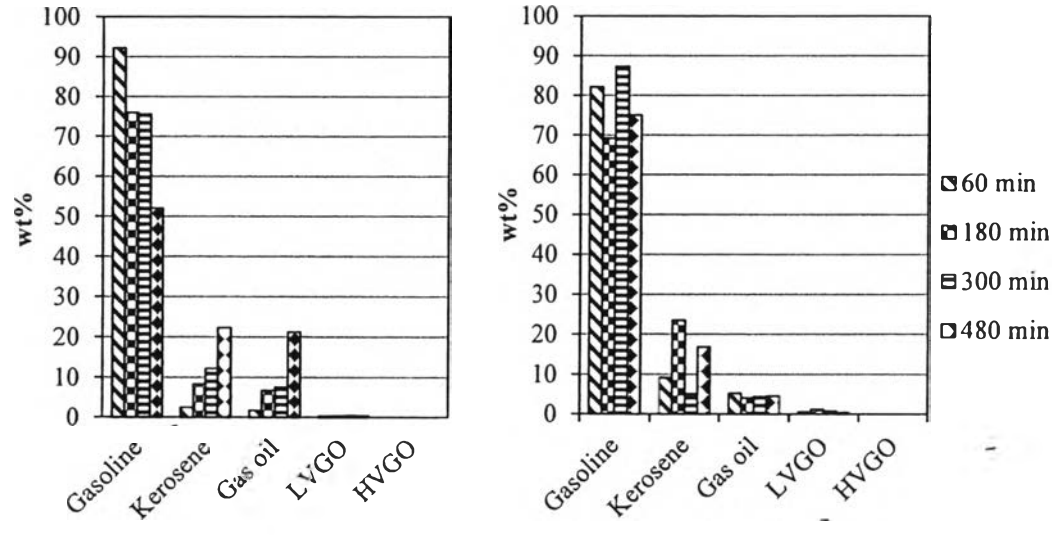

Figure 4.31 Petroleum fractions in oils from using 7 wt. % tin oxide doped SAPO-34 catalysts calcined at 400 C° (left) and 700 C°(right).

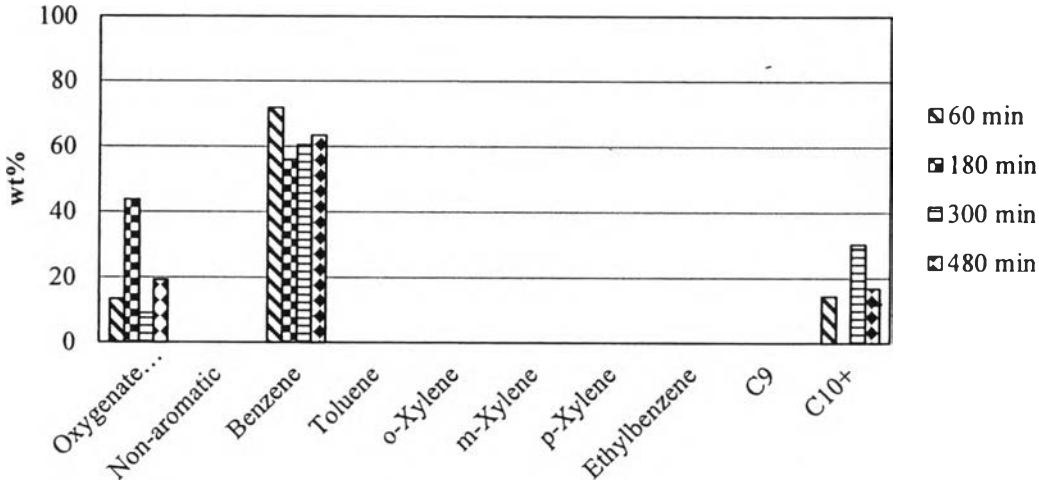

Figure 4.32 Composition of extracted oils from 7 wt.% tin oxide doped SAPO34 catalyst calcined at 400 °C.

Considering the extracted oil composition shown in Figures 4.32 and 4.33, the oil from using 7 wt. % of tin oxide-doped SAPO-34 catalyst with calcinations temperature of 400 C° highly consists of benzene, followed by oxygenate compounds and C10+ aromatics. The oxygenate compounds are mostly

pentanone and large molecules of ester while C10+ aromatics is mainly naphthanlene with branches. On the other hand, the obtained oils from using the modified SAPO-34 with calcinations temperature of 700 C° consist of oxygenate compound, and C10+ aromatics. Pentanone, Cyclopentanone, 2-methyl-ethane and 1,1-diethoxy are the main compounds in oxygenate compositions.

From the result, the calcination temperature has an influence on the oxidation state of tin oxide, changing from SnO_2 (Sn^{+4}) to SnO (Sn^{+2}), stable to metastable form due to high activation energy from high calcination temperature. From the result, both SnO (Sn^{+2}) and SnO_2 are responsible for butylenes formation. In addition, the result of oils shows that SnO (Sn^{+2}) on SAPO-34 is responsible for production of oxygenates, which the result is similar to when unsupported SnO was used displayed in Figure 4.5.

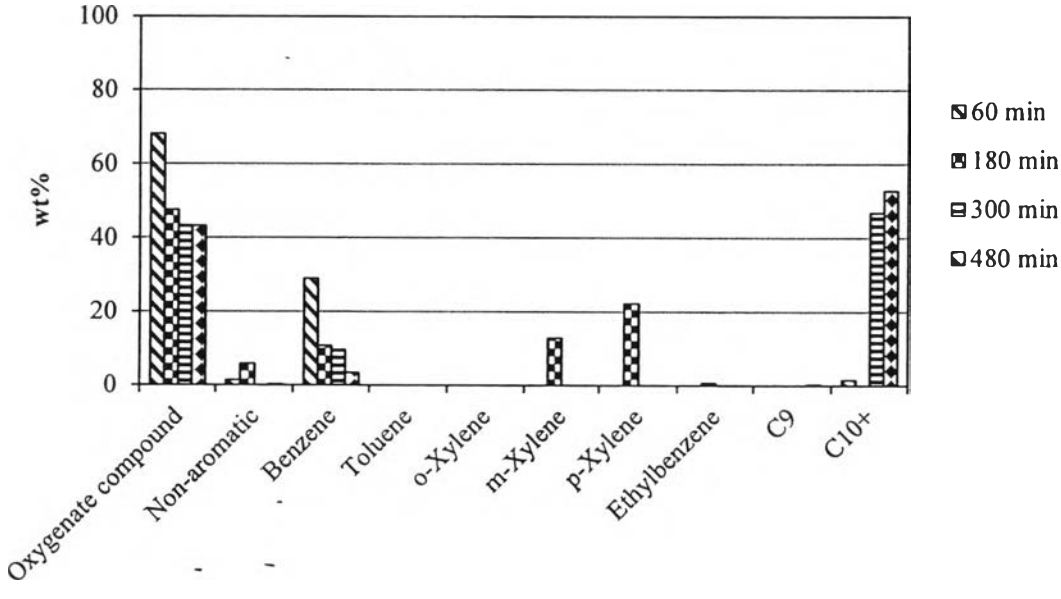

Figure 4.33 Composition of extracted oils from 7 wt.% tin oxide doped SAPO34 catalyst calcined at 700 °C.

4.2 Antimony

4.2.1 Pure Oxidation States of Antimony

4.2.1.1 Characterization of sole antimony catalysts

The XRD patterns of fresh and spent metallic antimony and antimony oxides are displayed in Figures 4.34 and 4.35. The peaks of metallic antimony can be detected at 2θ = 26.6°, 40.0°, 41.9°, 48.3°, and 51.5°. The peaks of Sb_2O_3 can be Observed at 2θ = 27.7°, 32.1°, 45.9°, 54.5° and 57.1° while Sb_2O_5 can be mainly detected at 2θ = 33.51°, 45.9°, and 48.73°. The XPS analysis of the fresh and spent catalysts was performed in order to observe the change of binding energy (BE) or oxidation state. After the binding energy calibration, the deconvolution of the Sn 3d was accomplished based on the BEs of metallic Sb (538 eV), Sb_2O_3 (539.6 eV), Sb_2O_5 (540.6 eV) (Garbassi, 1980). Figure 4.36 shows the fitted curves of metallic antimony (A), Sb_2O_3 (B) and Sb_2O_5 (C) catalysts before and after the dehydration of bio-ethanol. The composition of antimony species on the sole unsupported catalysts is shown in Appendix B. In Figure 4.36(A), the XPS spectra of fresh metallic antimony, which contain a peak located at 538 eV is assigned to Sb^0, accounted for 51.5%, and a peak located at 539.6 eV, and accounted for 49.5% is assigned to Sb_2O_3 (Sb^{+3}). Therefore, the commercial antimony is not pure at initial, containing 51.5% Sb^0 and 48.5% Sb_2O_3. Figure 4.36 (B) and (C) also indicates that the commercial unsupported Sb_2O_3 and Sb_2O_5 catalysts do not only contain its pure phase.

Table 4.4 Specific surface area and pore characteristics of antimony with different oxidation states

Metal Oxide	BET specific area	Pore Diameter	Pore Volume
	(m^2/g)	(nm)	(m^3/g)
Metal Sb	7.3	2.5	0.005
Sb_2O_3	5.3	10.5	0.02
Sb_2O_5	10.9	9.4	0.03

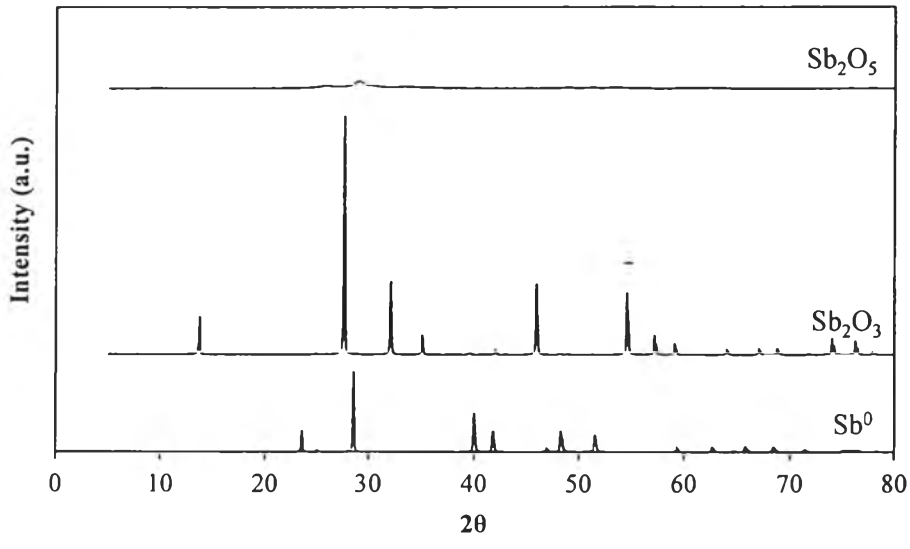

Figure 4.34 X-ray diffraction patterns of fresh antimony oxide catalysts with different oxidation states.

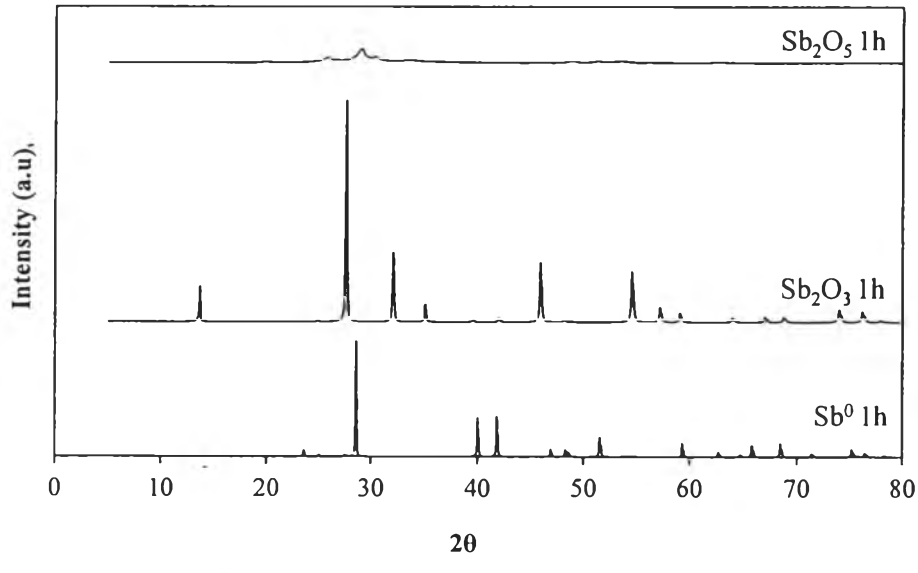

Figure 4.35 X-ray diffraction patterns of spend antimony oxide catalysts with different oxidation states.

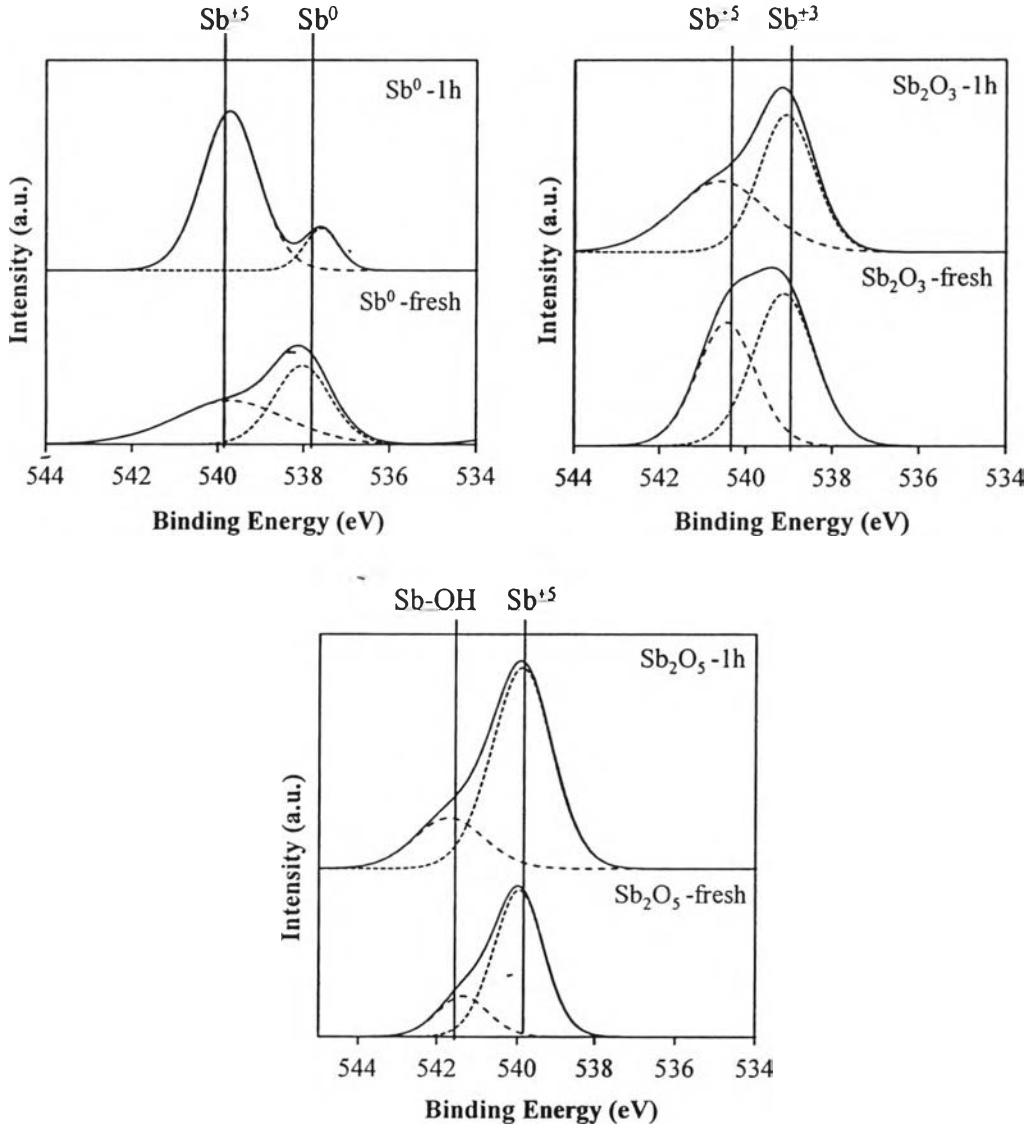

Figure 4.36 Sb $3d_{3/2}$ XPS spectra of (A) fresh and spent unsupported metallic antimony, (B) Sb_2O_3, and (C) Sb_2O_5.

The supported commercial Sb_2O_3 contains both Sb_2O_3 (Sb^{+3}) and Sb_2O_5 (Sb^{+5}) phases, accounted for 62% and 38%, respectively, whereas the unsupported Sb_2O_5 catalyst contains 78.4% of Sb_2O_5 (Sb^{+5}) and 21.6% of $Sb_2O_5 \cdot H_2O$. The result was also confirmed by the XRD peak at $2\theta=56.1°$. It is also found from the XPS results that the phases do not significantly change after 1 h of time-on-stream, except the commercial Sb^0 catalyst. After the reaction testing, the amount of Sb_2O_3 (Sb^{+3}) increases to 86.5%. It is known that antimony tends to be

oxidized when exposed to an oxidizing atmosphere. This indicates that, among all commercial antimony catalysts, metallic antimony is the most susceptible to oxidized during dehydration reaction.

4.2.1.2 Catalytic Activity of antimony oxides

The yield of extracted oils using all antimony catalysts is about 0.67% shown in Appendix A. Figure 4.37 displays the gas distribution. All catalysts decrease ethylene production, indicating that ethylene could undergo further reactions to form propylene, cooking gas, and butylenes. Surprisingly, the selectivity of butylenes is the highest with using metallic antimony, whereas Sb_2O_5 (Sb^{+5}) gives the highest propylene and cooking gas.

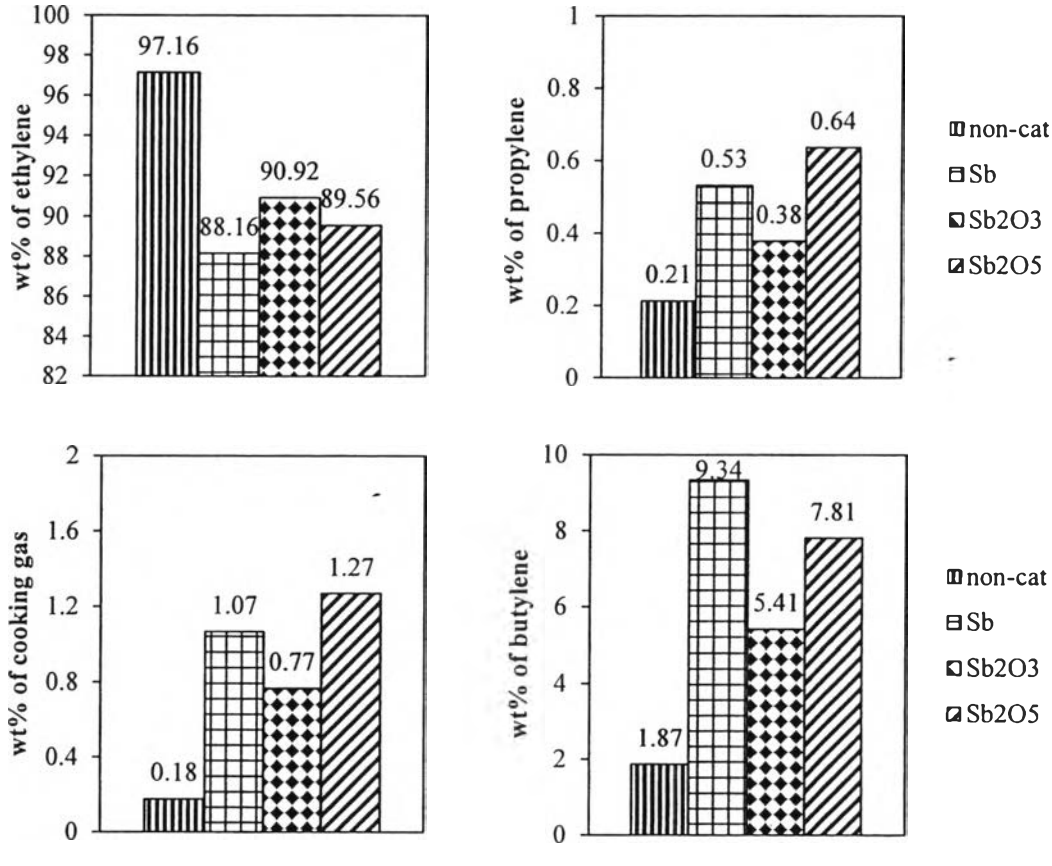

Figure 4.37 Weight percentage of ethylene, propylene, cooking gas and butylenes in the gas products from using metallic antimony, Sb_2O_3 and Sb_2O_5 catalysts.

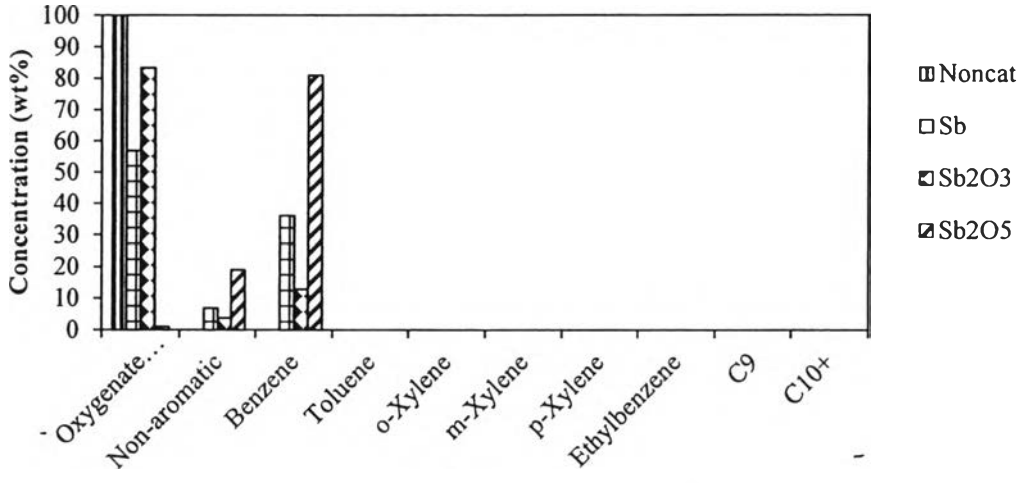

Figure 4.38 Composition of oils using metallic antimony, Sb_2O_3 and Sb_2O_5 catalysts.

This may be due to the contamination of Sb^{+5} in metallic antimony. Since Sb+5 is formed in metallic antimony, Sb^{+5} may help to convert ethanol to form ethylene and then butylenes, but it is not strong enough to form benzene through reaction pathway. Therfore, the selectivity of butylenes is lower and the selectivity of benzene is higher with using Sb_2O_5, compared to metallic antimony.

The oil compositions obtained from unsupported commercial metallic Sb, Sb_2O_3 and Sb_2O_5 shown in Figure 4.38 are remarkably different. The main products in oils using either metallic antimony or Sb_2O_3 catalysts are oxygenates, non aromatics and benzene, whereas only non-aromatics and benzene was the main components with using Sb_2O_5. According to the acid property of metal oxides, antimony oxide is non-metal, which shows acidic characters. Since acid strength also increases with the number of oxygen substitution on the central atom; therefore, Sb_2O_5 (Sb^{+5}) that has the highest oxidation state favors hydrocarbon formation rather than oxygenates. However, it is noticed that metallic antimony gives both oxygenates and hydrocarbons. It is because the commercial metallic antimony is contaminated with Sb_2O_5 (Sb^{+5}) phase.

The result of oil composition shows that Sb_2O_5 (Sb^{+5}) is responsible for propylene and benzene formation, whereas Sb^0 and Sb_2O_3 (Sb^{+3}) might selective to oxygenate production due to the lowest oxygen substitution.

4.2.2 Interaction between Sb^0 and SAPO-34

In this part, metallic antimony was mixed with SAPO-34, followed by hydrogen treatment in order to create the interaction between metal and support. The XPS analysis of fresh and spent catalysts was performed in order to observe the interaction between the metal and the SAPO-34 support from the change of binding energy (BE) or oxidation state. After the binding energy calibration, the convolution of the Sn 3d was accomplished based on the BE of metallic Sb (538 eV), Sb_2O_3 (539.6 eV), Sb_2O_5 (540.6 eV) (Garbassi, 1980). Figure 4.39 shows the fitted curve of $5Sb^0$ SAPO-34 before and metallic antimony. The Sb $3d_{3/2}$ XPS spectra of metallic antimony doped on SAPO-34 are located at 538.2 eV, which shifts to a slightly higher BE than that of pure Sb^0. This infers that there is an interaction between metal and support. After catalytic testing, the surface compostion on SAPO-34 changes to 86.5% Sb_2O_5 (Sb^{+5}) and 15.9% Sb^0.

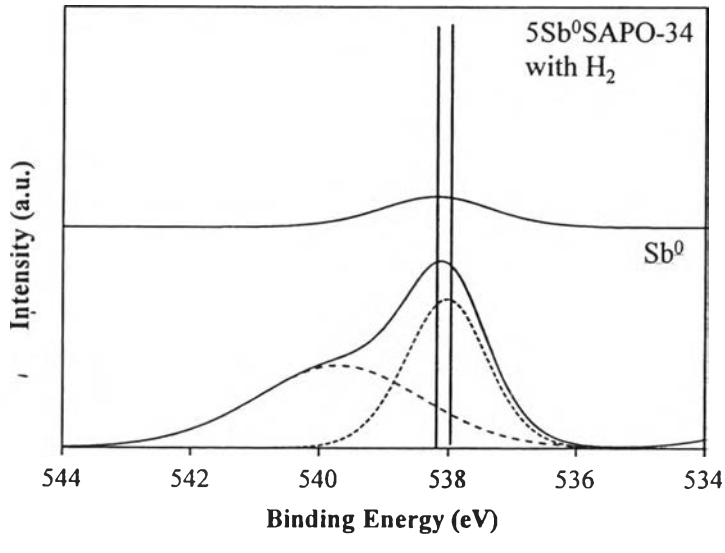

Figure 4.39 Sb $3d_{3/2}$ XPS spectra of fresh and spent $5Sb^0$/SAPO-34.

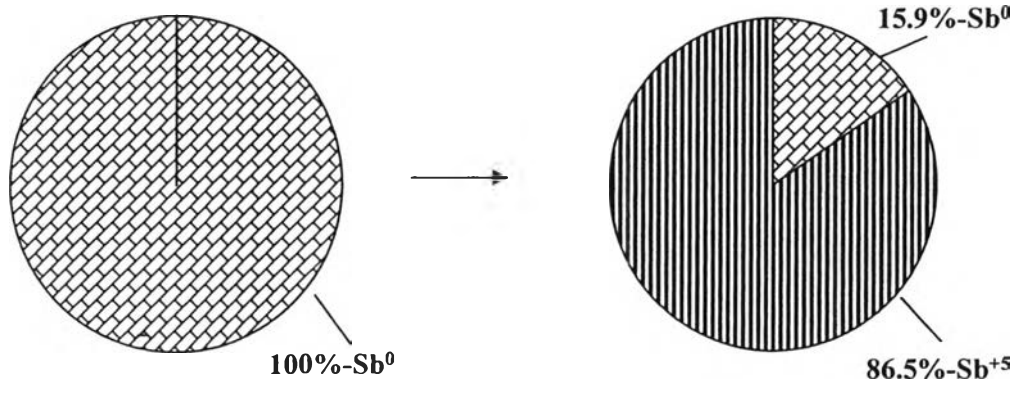

Figure 4.40 Antimony species of $5Sb^0$ SAPO-34 before and after reaction.

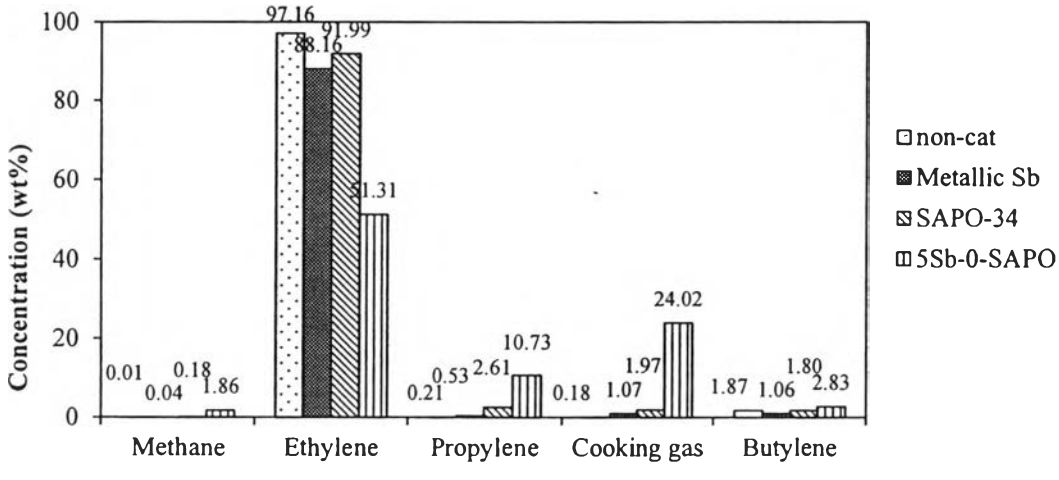

Figure 4.41 Weight percentage of ethylene, propylene, cooking gas and butylenes in the gas product using $5Sb^0$/SAPO-34.

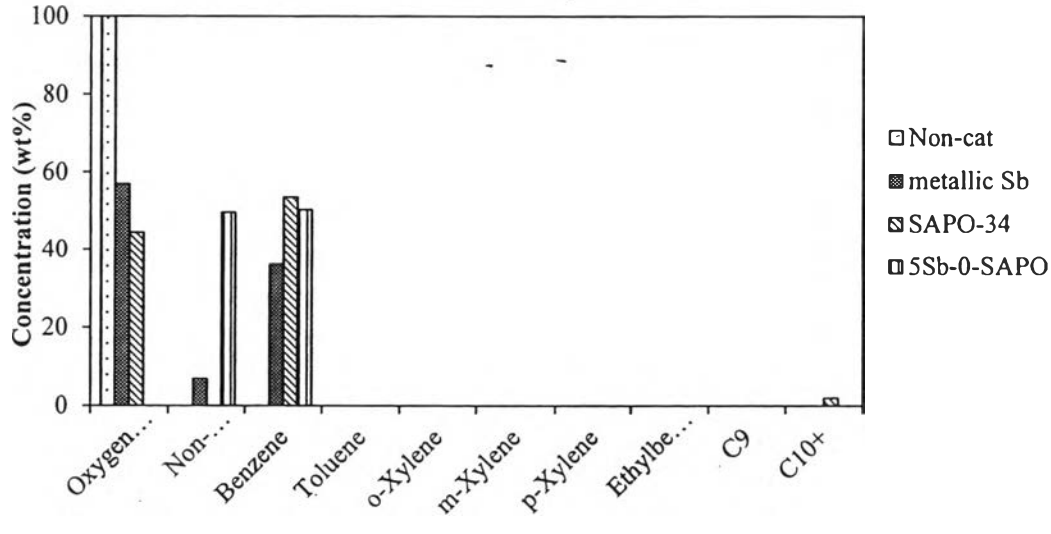

Figure 4.42 Composition of oils using $5Sb^0$/SAPO-34.

The reason for the change of oxidation state of $5Sb^0$/SAPO-34 is the same as that of pure metallic antiomony. Figure 4.41 shows the gas selectivity of ethylene, propylene, cooking gas and butylenes. The selectivity of cooking gas from using Sb^0/SAPO-34 is significantly higher than that of Sb^0. This indicates that metallic antimony not only has dehydrogenation-hydrogenation property, but also is highly dispersed on SAPO-34. Otherwise, metallic antimony would not have given the cooking gas as high as reported. Therefore, the interaction between Sb^0 and SAPO-34 with appropriate pore constraint and acidity obviously enhances cooking gas formation.

The main products in oils using $5Sb^0$/SAPO-34 displayed in Figure 4.42 consist of only non-aromatics and benzene. It is also noticed that oil yield slightly increases. Among the non-aromatics obtained from $5Sb^0$/SAPO-34, hexane, cyclohexane, pentene, cyclopentane and cyclopentene with branches are the main components. Both saturated and unsaturated compounds were observed in non-aromatics. However, the selectivity of benzene using $5Sb^0$/SAPO-34 remains constant, comparing to using SAPO-34. This infers that metallic antimony may slightly enhance the aromatization reaction.

From the result, it is found that there is an interaction between metallic antimony and SAPO-34, which is supported by XPS result. SAPO-34 also help metallic antimony to be highly dispersed, resulting in significantly higher selectivity of cooking gas, compared to sole metallic antimony.

4.2.3 Sb_2O_x/SAPO-34

Figures 4.45 and 4.46 show the changes of surface composition of between 5 and 7 wt% Sb_2O_x on SAPO-34 before and after the catalytic test as time-on-stream. Since Sb $3d_{5/2}$ is superimposed with O 1s; therefore, the peak position of Sb 3d3/2 is used to determine the oxidation of antimony oxide instead. The fitting procedure was performed by considering the binding energy of Sb_2O_3 (539.6-539.9) and Sb_2O_5 (540.7-540.9) as follows. From XPS analysis, the peaks of Sb $3d_{3/2}$ of both catalysts in Figures 4.43 and 4.44 show fitting curve results. It is found that both of the catalysts contain mixed oxides with two oxidation states; namely, Sb_2O_3 and

Sb_2O_5. However, the amount of Sb^{+3} increases when the percent loading of antimony oxide increases, indicating that the antimony oxide on SAPO-34 prefers to stay in the form of Sb_2O_3 with increasing antimony loading.

The higher formation of Sb_2O_3 can be explained from the antimony specie result of sole antimony oxide. From Figure 4.36, it is notice that both metallic antimony and Sb_2O_3 contain Sb^{+5} species, indicating Sb^{+5} is the more stable oxidation state number than Sb^{+3}. At 5wt% Sb_2O_x loading, antimony oxide might be more highly dispersed than that of 7wt% antimony, which can be observed from the compositions in Figure 4.45. The percentages of Sb^{+3} and Sb^{+5} stay closely. On the other hand, the percentages of Sb^{+3} and Sb^{+5} of 7wt% Sb_2O_x-doped SAPO-34 stay more separately. This means that due to higher loading percentage and larger cluster, Sb^{+3} species, which is less stable, can be able to maintain its structure.

Figure 4.47 displays the gas selectivity of ethylene, propylene, cooking gas and butylenes from the dehydration of bio-ethanol. The result shows that, initially, 5 wt.% loading gives a higher selectivity of propylene, cooking and butylenes than those of 7wt.% loading, except for the selectivity of ethylene. This may be due to the different acid strength. From the XPS result, this can be inferred that the surface composition of antimony oxides effects the product distribution. 5wt.% of antimony oxide supported catalyst contains a higher amount of Sb^{+5} species more than that of 7wt.% one, resulting in higher acid strength and the higher selectivity of propylene, cooking gas and butylenes. After, 60 min of reaction time, it is observed that the selectivity of ethylene produced from 7wt.% of antimony increases significantly while the amount of the other gases decreases almost half, compared with 5 wt.% loading at the same time-on-stream. As the time-on-stream increases, the selectivity of gas, except ethylene and butylenes decreases. This can be explained that the increase of Sb^{+3} species results in lower acid strength. Butylenes might not be able to be converted to bigger hydrocarbons.

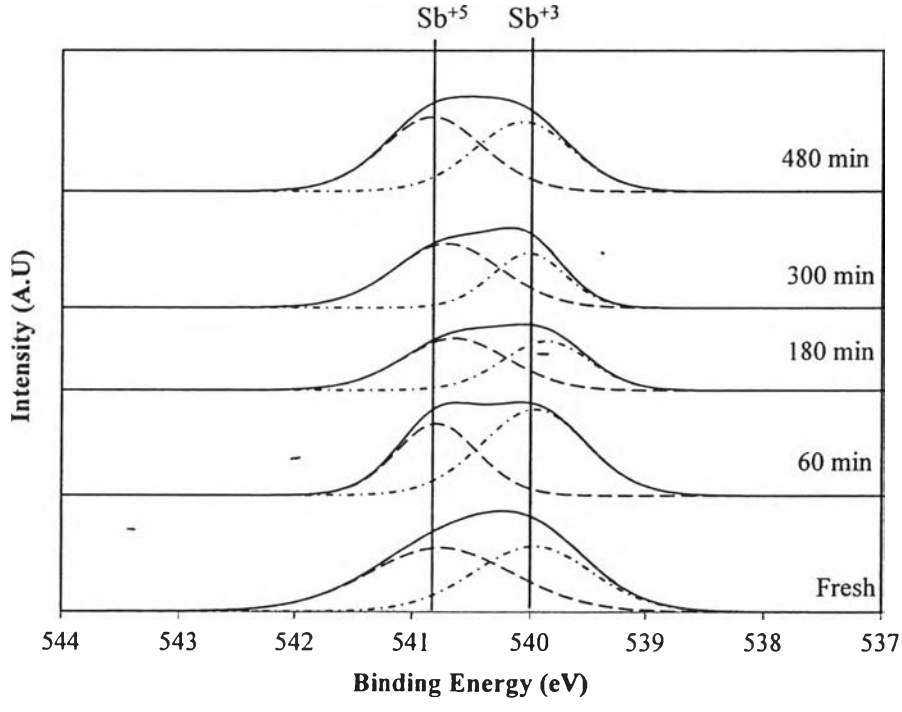

Figure 4.43 XPS spectra of 5wt% of antimony oxide-doped SAPO-34 before and after catalyst performance testing.

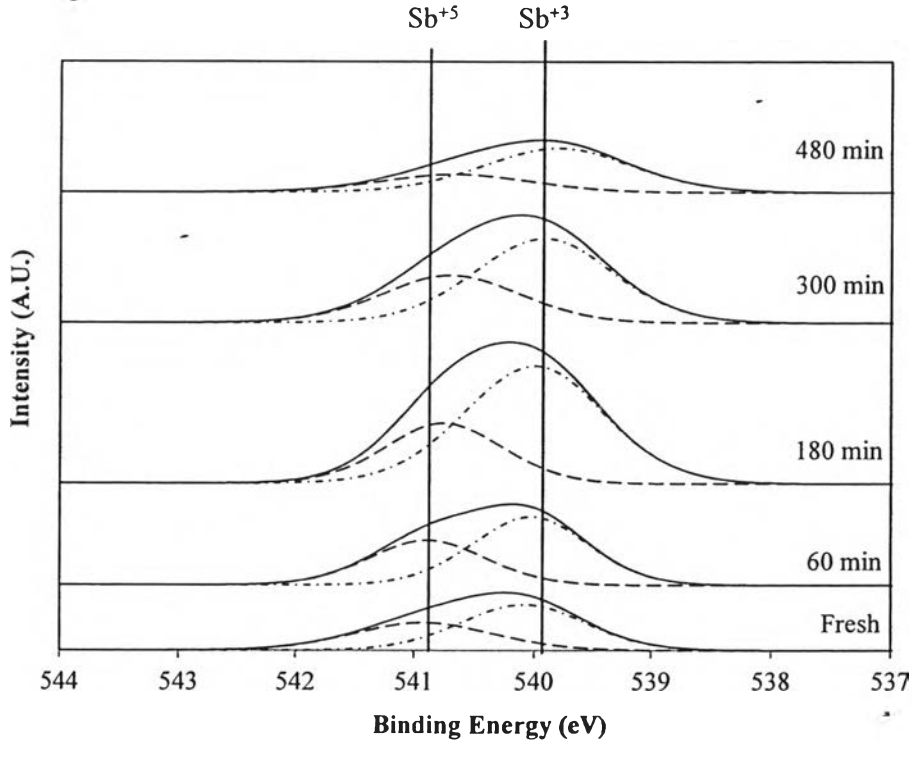

Figure 4.44 XPS spectra of 7 wt% of antimony oxide-dopedSAPO-34 before and after catalyst performance testing.

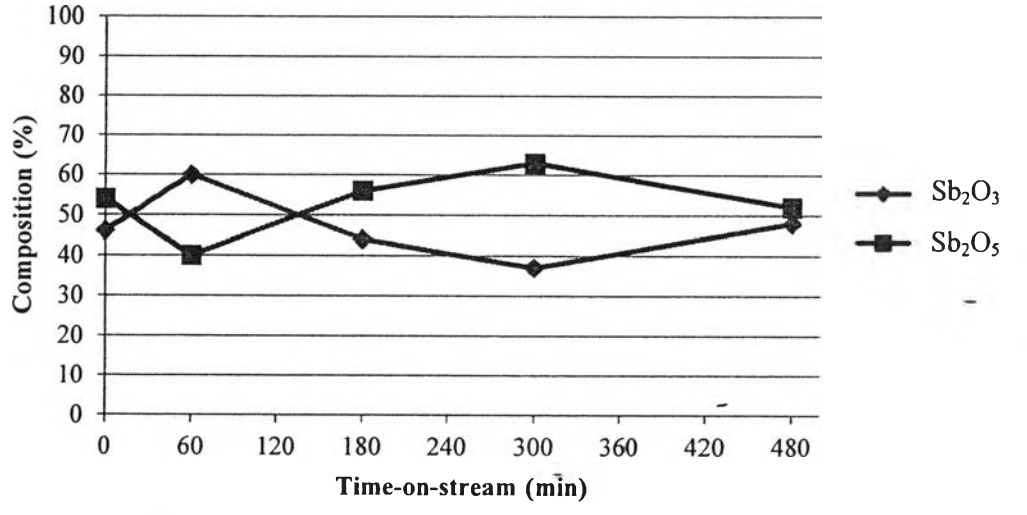

Figure 4.45 Changes of Species and compositions of antimony oxides on 5 wt.% tin oxide-doped SAPO-34 calcined at 400 °C.

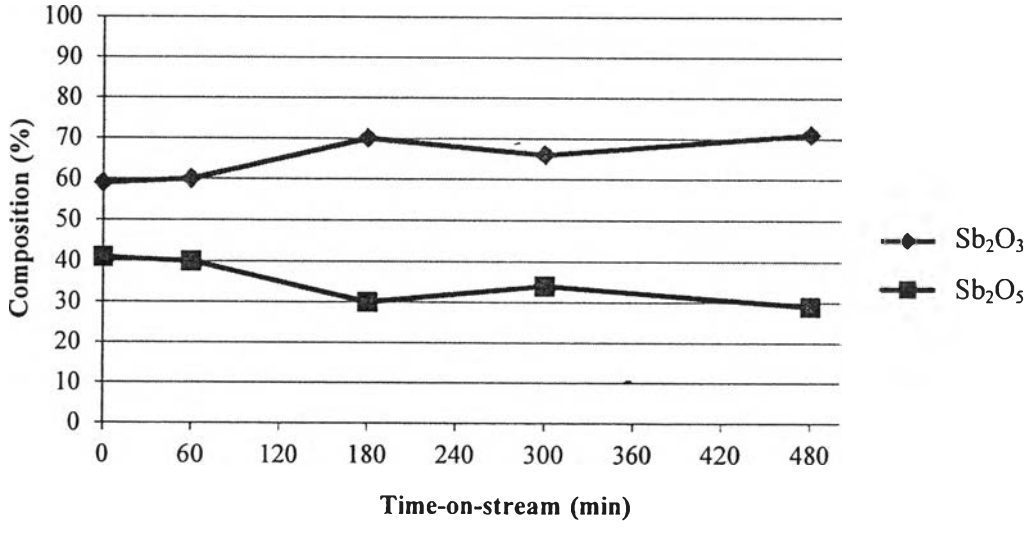

Figure 4.46 Changes of Species and compositions of antimony oxides on 7 wt.% tin oxide-doped SAPO-34 calcined at 400 °C.

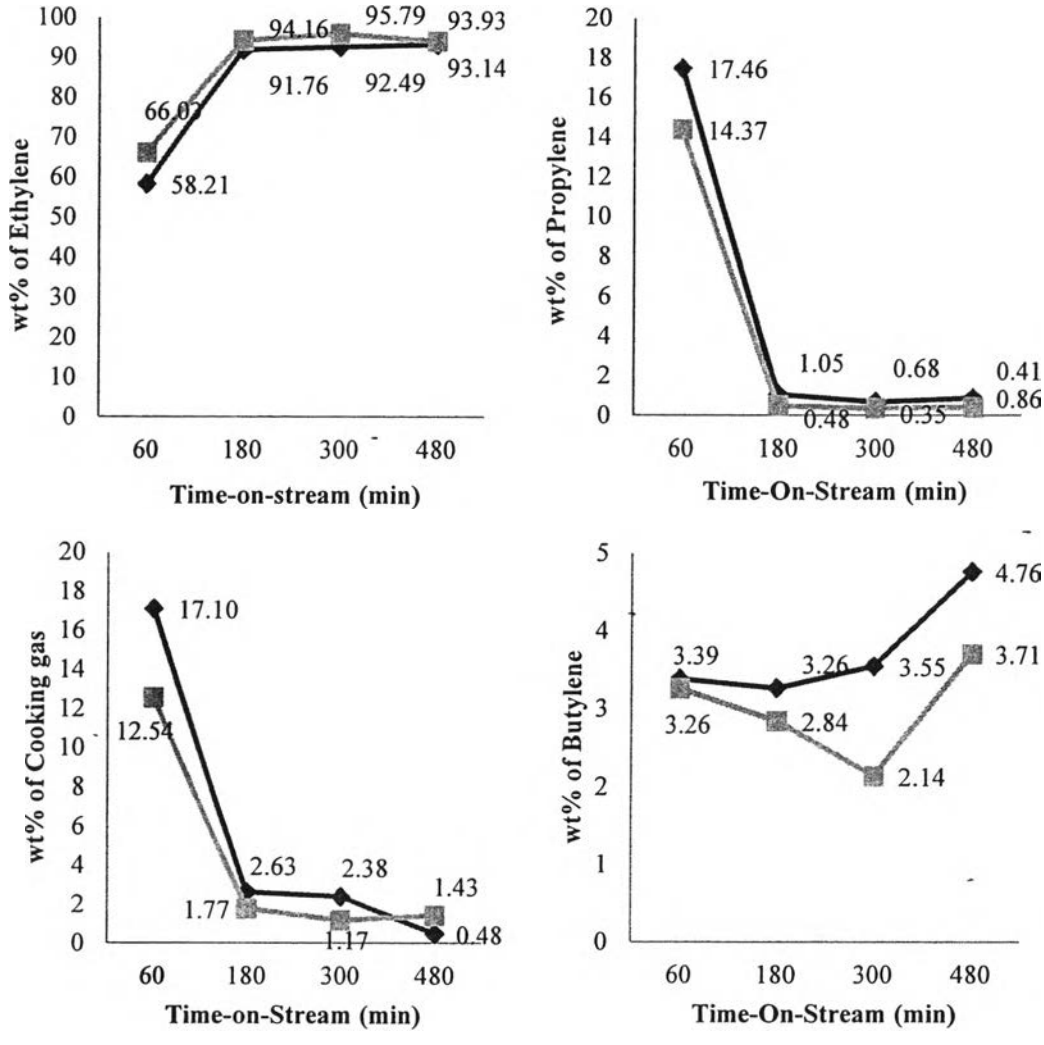

Figure 4.47 Weight percentage of ethylene, propylene, cooking gas and butylenes in gas phase from 5wt% (♦) and 7wt% (■) of antimony oxide on SAPO-34.

In addition, the petroleum fractions of 5 and 7 wt. % antimony oxide doped on SAPO-34 are displayed in Figures 4.48 and 4.49, respectively. The TBPs of extracted oil mainly fall in to gasoline range. For 5 wt. % loading, kerosene and gas oil in the extracted oil increase to 10 wt. % and 30 wt. %, respectively, with increasing time-on-stream. The same trend of petroleum fraction is also shown in 7 wt. % of Sb_2O_x-doped SAPO-34. The composition of kerosene range in the extracted oil increase up to 40 wt% when compared with that of the unmodified catalyst. This indicates that the heavy petroleum fractions such as kerosene and gas oil increase when the Sb_2O_x was added.

Figures 4.50 and 4.51 show the liquid composition from the catalytic dehydration of bio-ethanol. The derived oils from both catalysts consist of oxygenate compounds, benzene and, especially, C10+ aromatics. It is observed that 5wt. % of Sb_2O_x-doped SAPO-34, which consists of a higher amount of Sb^{+5} component, shows 40 wt.% lower selectivity of benzene than that of 7wt. % Sb_2O_x loading at 60 min of time-on-stream. However, the 5 wt.% of antimony loading on SAPO-34 is highly selective to the formation of C10+ aromatics, even though the oil yield stays constant. As the time-on-stream increases, the changes of C10+ aromatic selectivity from using 5wt% Sb_2O_x-doped SAPO-34 is similar to those of Sb^{+5}, while the changes of Sb^{+5} in 7wt% Sb_2O_x-doped SAPO-34 follow the trend of benzene formation. In addition, it was found that the oil yield from using 5wt% Sb_2O_x-doped SAPO-34 was higher than that of 7wt%. This means that the increase of antimony loading from 5 wt.% to 7 wt.% influences significantly on the liquid product distribution, rather than an increase of oil-yield.

From the results of both gas and oil, it is found that the changes of Sb_2O_5 (Sb^{+5}) govern the gas selectivity of propylene, butylenes and benzene formation, whereas Sb_2O_3 (Sb^{+3}) is selective to oxygenates formation. The result of gas selectivies of modified catalysts and sole metal oxides are similar. However, highly dispersed Sb_2O_5 (Sb^{+5}) on SAPO-34 could enhance the conversion from benzene to C10+ aromtics through dehydration reaction pathway, which can also be observed from the higher shift of binding energy.

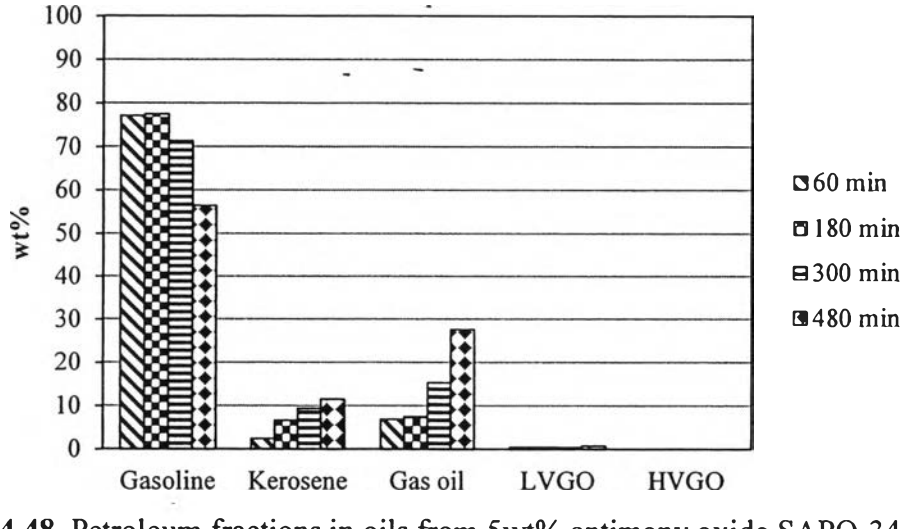

Figure 4.48 Petroleum fractions in oils from 5wt% antimony oxide SAPO-34.

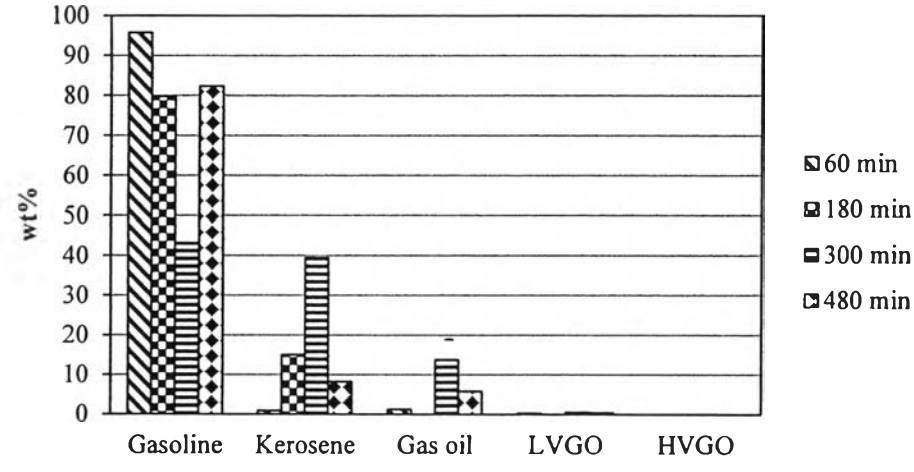

Figure 4.49 Petroleum fractions in oils from 7wt% antimony oxide SAPO-34.

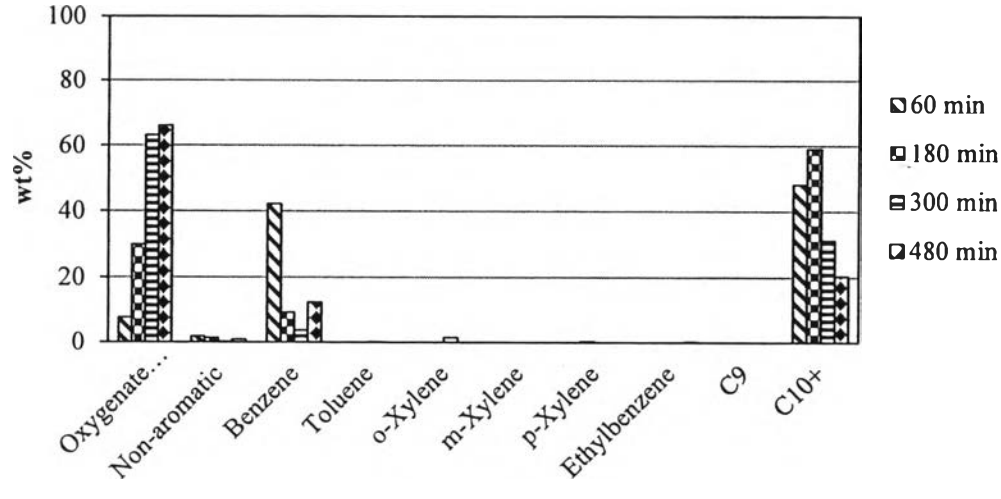

Figure 4.50 Composition of oils from 5 wt.% of antimony oxide SAPO-34.

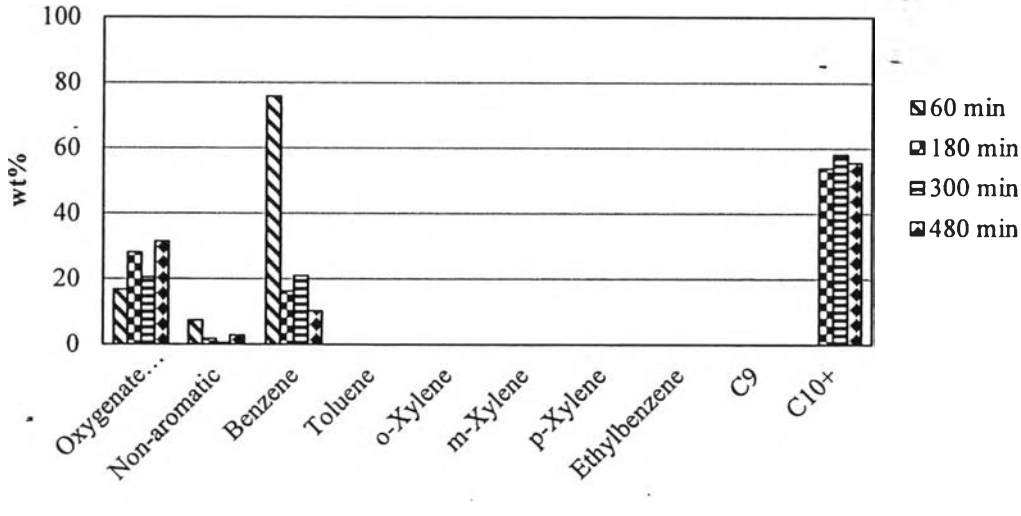

Figure 4.51 Composition of oils from 7 wt.% of antimony oxide SAPO-34.

The effect of calcinations temperature was observed in order to see the change of product distribution on catalytic dehydration of bio-ethanol along with the change of antimony species. The antimony oxide species present on SAPO-34 catalysts when calcined at 400 C° and 700C°, were examined using XPS. After the curve fitting procedure, the XPS spectrum of fresh catalysts indicates a shift of the Sb $3d_{3/2}$ binding energy toward lower values as the calcination temperature increases to 700C°. The fitting procedure was performed by considering the binding energy of Sb^{+3}(Sb_2O_3) (539.6-539.9) and Sb^{+5} (Sb_2O_5) (540.7-540.9) as follows. The species of antimony oxide and binding energy are shown in Figures 4.53, 4.54, and Appendix C. Both of catalysts contain a mixture of antimony oxides. With 5SbSAPO-34 calcined 400 °C contains antimony with oxidations of +3 and +5, accounted for 45.7% and 54.3%, respectively. On the other hand, 5SbSAPO-34 calcined at 700 °C also contains antimony with oxidations of +3 and +5, but accounted for 35.1% and 64.5%, respectively. From Figure 4.52, the surface composition of antimony oxides with the oxidation +3 increases continuously to 180 min time-on-stream, and then decreases. It is noticed that the change of oxidation state of antimony versus time-on-stream of 5 wt% antimony oxide calcined at 700 °C is similar to that of 5 wt.% antimony oxide-doped SAPO-34 calcined at 400 °C. It was also mentioned that Sb_2O_3 can be oxidized back and forth (Mestl *et al.*, 1994). This infers that antimony oxides doped on SAPO-34 calcined at 400 °C are more active than that of calcined at 700 °C.

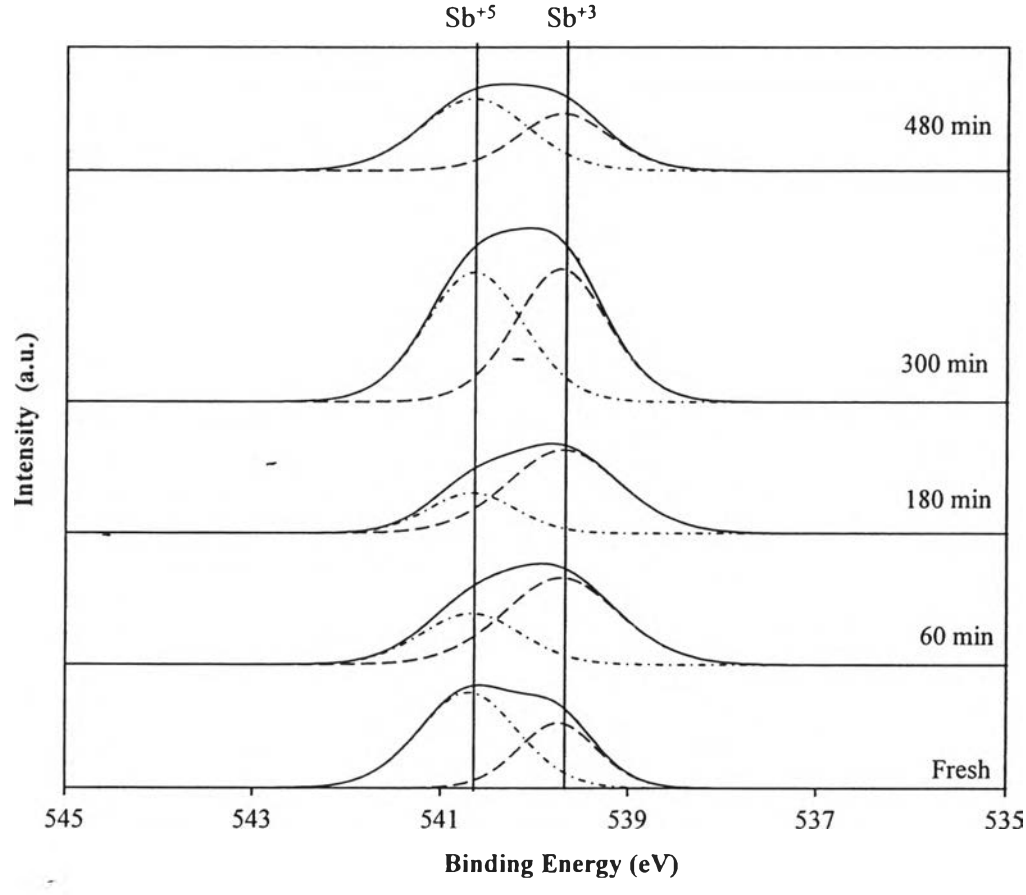

Figure 4.52 XPS spectra of fresh and spent 5SbSAPO34 calcined at 700 °C.

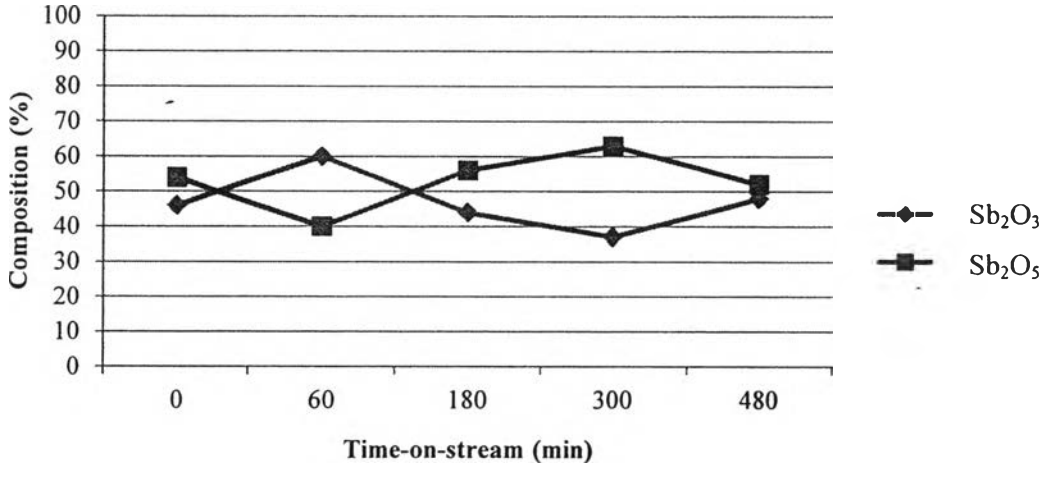

Figure 4.53 Changes of Species and composition of antimony oxides on 5 wt.% tin oxide-doped SAPO-34 calcined at 400 °C.

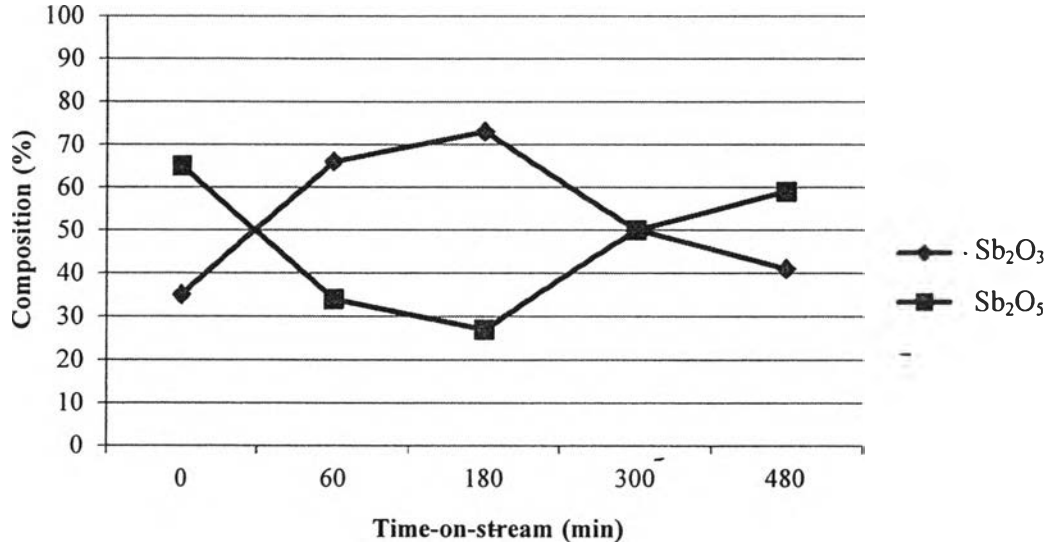

Figure 4.54 Changes of Species and compositions of antimony oxides on 5 wt.% tin oxide-doped SAPO-34 calcined at 700 °C.

The gas and oil yields are shown in Appendix A. In Figure 4.55, for 5SbSAPO-34 calcined at 700 °C, it seems that the gas selectivity of propylene, cooking gas and butylenes follows the change of Sb_2O_5. This confirms that the selectivity of gas may be governed by Sb_2O_5 (Sb^{+5}). Because of less activeness, the formations of gases other than ethylene need higher acid strength, which is an antimony oxide at a high oxidation state. In addition, It was found that the oil yield and petroleum fractions shown in Figure 4.56 (left) obtained from 5SbSAPO-34 calcined at 400 °C increase more rapidly and those of 5SbSAPO-34 calcined at 700 °C shown on Figure 4.56 (right). This indicates that antimony oxide with calcination temperature 400 °C is more active than 5SbSAPO-34 calcine 700 °C.

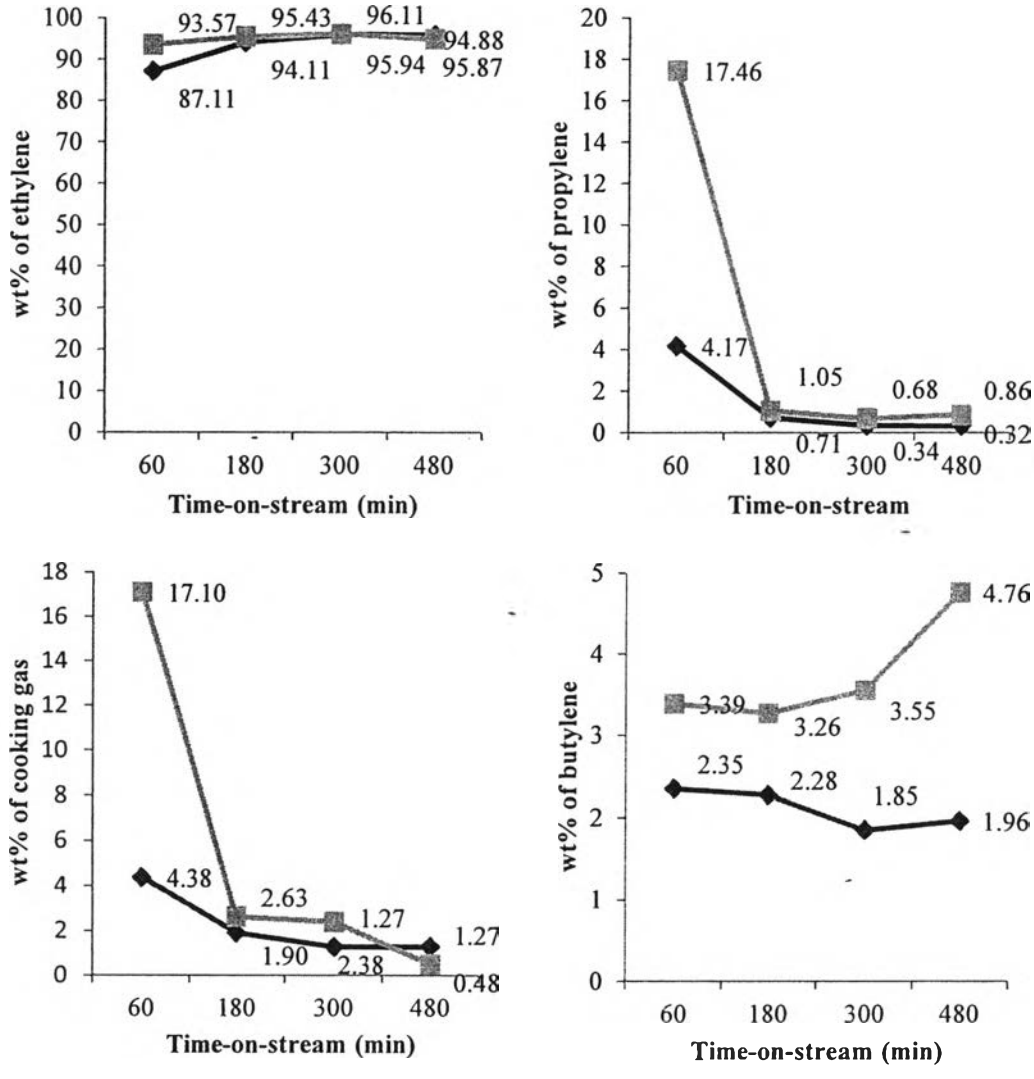

Figure 4.55 Weight percentage of ethylene, propylene, cooking gas and butylenes from 5 wt. % antimony oxide on SAPO-34 calcined at 400 C°(■) and 700C°(♦), respectively.

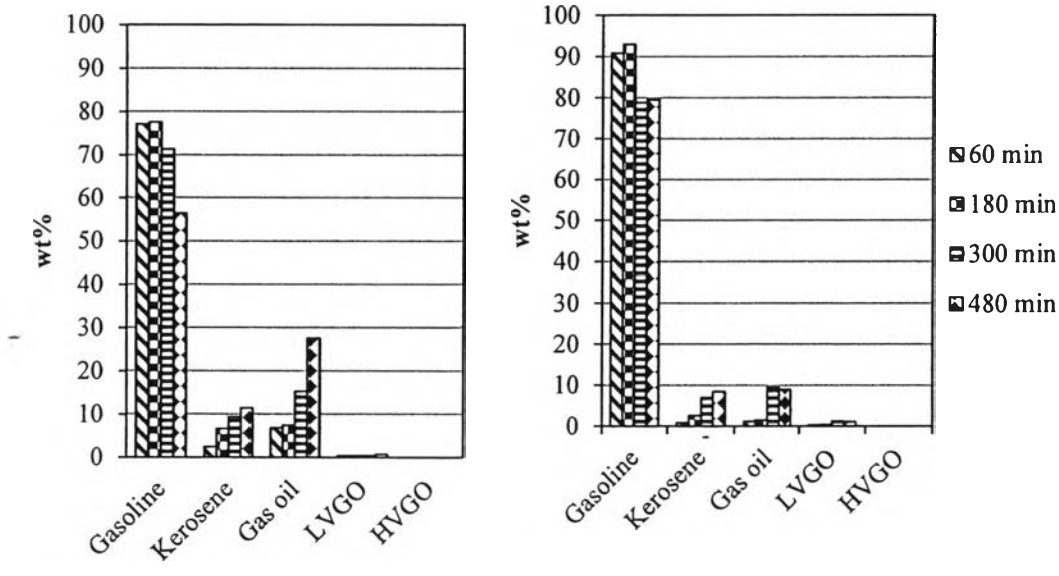

Figure 4.56 Petroleum fractions in oils from using 5 wt. % antimony oxide-doped SAPO-34 catalysts calcined at 400 C° (left) and 700 C°(right).

The compositions of extracted oil of 5SbSAPO-34 calcined at 400 °C and 700 °C displayed in Figures 4.57 and 4.58, respectively. It was found that oils from both catalysts contain mainly oxygenates and benzene, except 5SbSAPO-34 calcined at 400 °C that contains C+10 aromatics. This may be because, at the calcination temperature of 700 °C, the loaded antimony oxides may accumulate themselves, and act as individual antimony oxides. It was observed from the XRD study shown in Appendix C that the peaks of 5SbSAPO-34 calcined at 400 °C are sharper and broader, located at the similar binding energies of sole Sb_2O_3 and Sb_2O_5. This infers that antimony oxides from the catalyst calcined at 400 °C are more highly dispersed that the one calcined at 700 °C. Therefore, the selectivity of oxygenates increases with the increase of Sb_2O_3, which corresponds to the oxygenate result obtained from using pure Sb_2O_3.

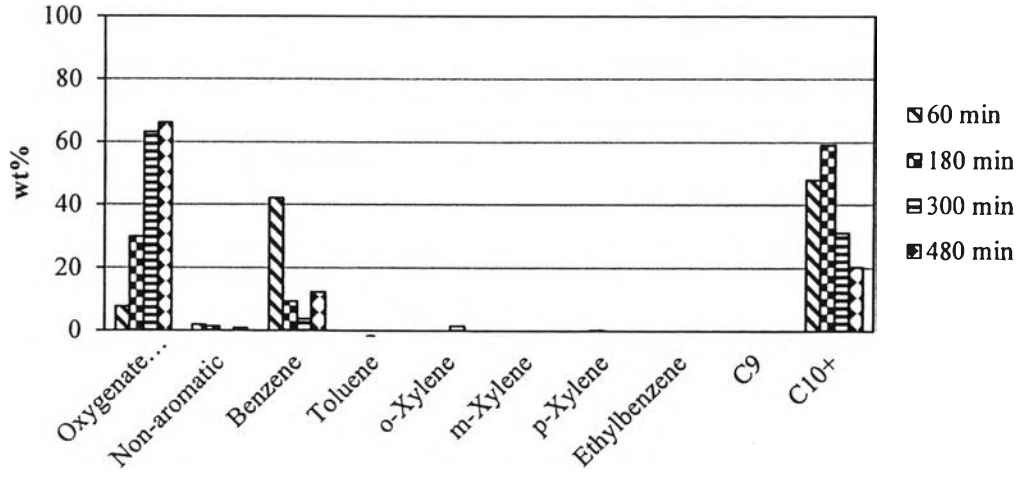

Figure 4.57 Composition of oils from 5 wt.% of antimony oxide on SAPO-34 calcined at 400 C°.

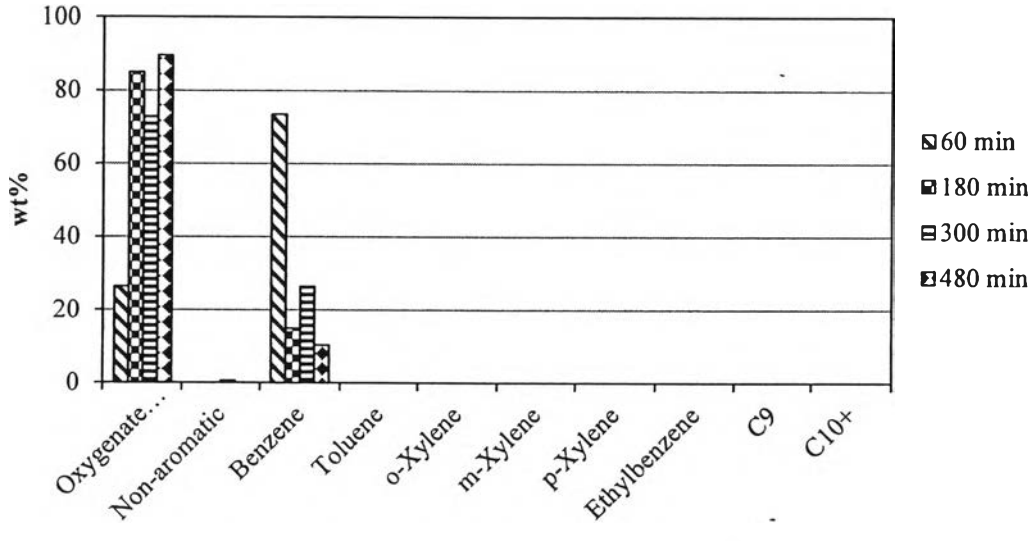

. **Figure 4.58** Composition of oils from 5 wt.% of antimony oxide on SAPO-34 calcined at 700 C°.

The changes of antimony species on 7wt% Sb_2O_x-doped SAPO34 with calcination temperatures of 400 °C and 700 °C were observed. After the curve fitting procedure, the XPS spectra of fresh catalysts indicate a shift of the Sb $3d_{3/2}$ binding energy toward lower values as the calcination temperature increases to 700C°. The fitting procedure was performed by considering the binding energy of Sb_2O_3 (539.6-539.9) and Sb_2O_5 (540.7-540.9) as follows. The species of antimony

oxide and binding energy are shown in Figures 4.60, 4.61 and Appendix C. Both catalysts contained mixed oxidation state of antimony oxides. 7SbSAPO-34 calcined at 400 °C contains Sb_2O_3 and Sb_2O_5, accounted for 59.4% and 40.6%, respectively. On the other hand, 7SbSAPO-34 calcined at 700 °C contains also Sb_2O_3 and Sb_2O_5, but accounted for 70.5% and 29.5%, respectively. It was noticed that Sb_2O_3 increases, and the binding energy is lower to the value of pure Sb_2O_3 (Garbassi, 1980).

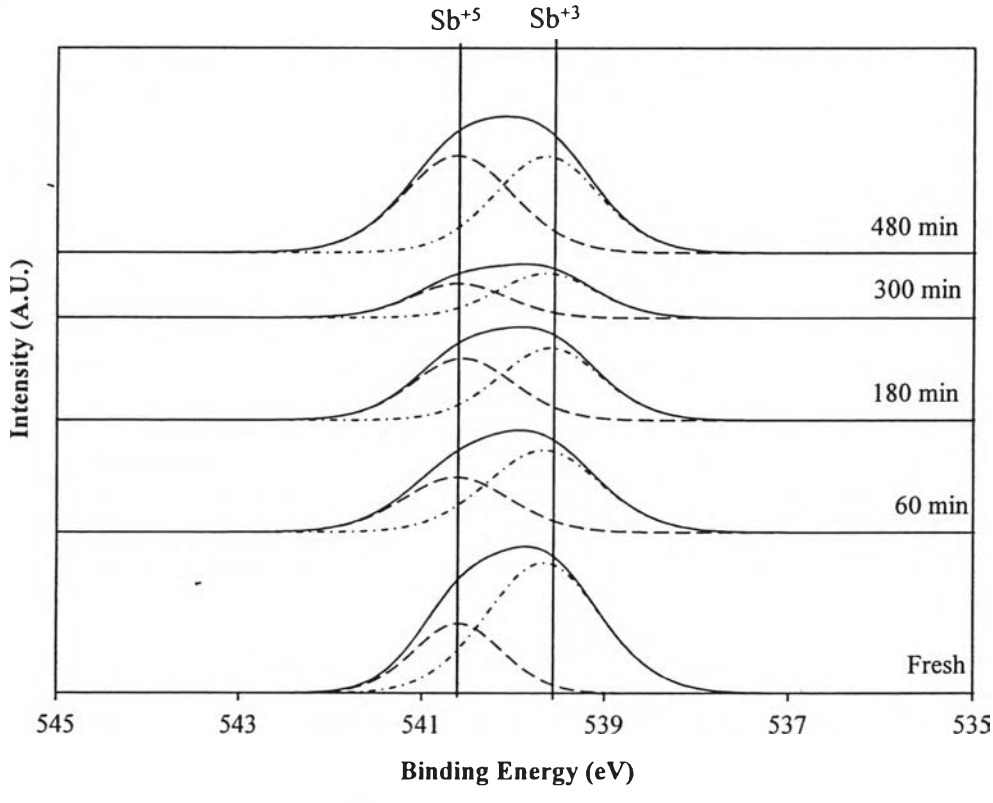

Figure 4.59 XPS spectra of fresh and spent 7SbSAPO34 calcined at 700 °C.

It is suggested that antimony oxides deposited on SAPO-34 may accumulated themselves and can stay in an unstable form (Sb_2O_3) with increasing calcination temperature due to higher activation energy. According to Irmawati *et al.* (2004), it was reported that the increase of calcination temperature can promote the crystallinity of antimony oxide. The gas and oil yields are shown in Appendix A. For 7SbSAPO-34 calcined at 700 °C, it seems that the gas selectivity of butylenes follows the change of Sb_2O_5 as similarly as that in 5SbSAPO-34 calcined at 700 °C.

This confirms that the selectivity of gas may be governed by Sb_2O_5 when calcined at 700 °C.

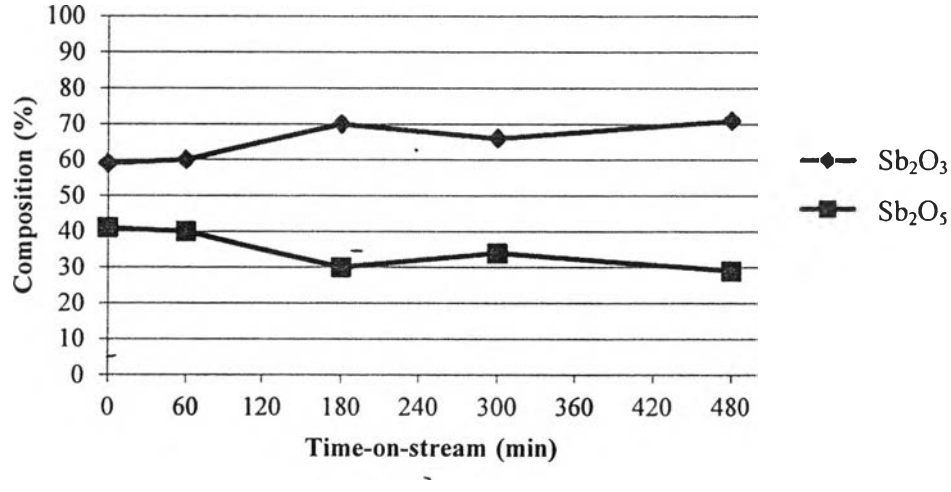

Figure 4.60 Changes of Species and compositions of antimony oxides on 7 wt.% antimony oxide-doped SAPO-34 calcined at 400 °C.

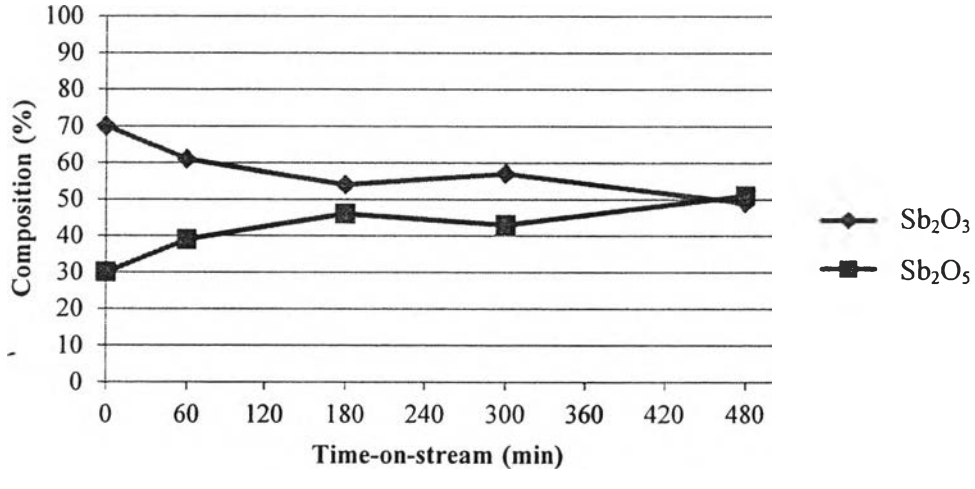

Figure 4.61 Changes of Species and compositions of antimony oxides on 7 wt.% antimony oxide-doped SAPO-34 calcined at 700 °C.

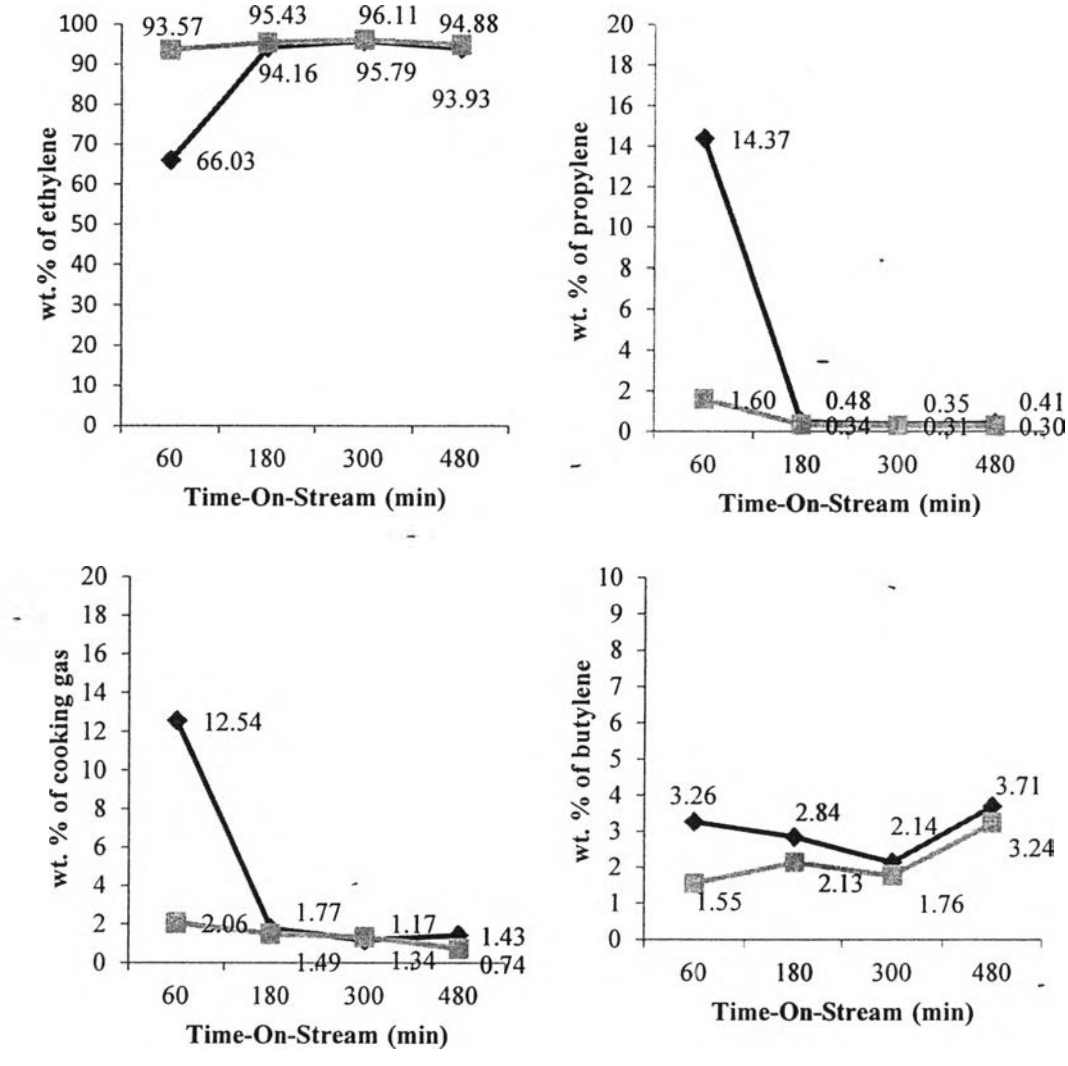

Figure 4.62 Weight percentage of ethylene, propylene, cooking gas and butylenes from using 7 wt. % antimony oxide on SAPO-34 calcined at 400 C°(♦) and 700C°(■), respectively.

In addition, it was found that the oil yield and petroleum fractions shown in Figure 4.63 (left) obtained from 7SbSAPO-34 calcined at 400 °C increase more rapidly than those of 7SbSAPO-34 calcined at 700 °C shown on Figure 4.63 (right). This indicates that antimony oxidea at calcination temperature 400 °C are more active than those of 5SbSAPO-34 calcined at 700 °C. For the oil composition, with the calcination temperature of 700 °C, oxygenates, non-aromatics and benzene are the main components, whereas C+10 aromatics is found using 7SbSAPO-34 calcined at 400 °C. This indicated that there is a synergistic effect between highly-

disperse antimony oxides. However, at the calcination temperature at 700 °C, the agglomerate antimony oxide might inhibit the formation of hydrocarbons. The result is also similar to that of sole antimony oxide.

From the result, the increase of calcination temperature have the influence on the surface composition of Sb_2O_x-doped SAPO-34; that is, the content of metastable form (Sb_2O_3) increases or accumulates itself as sole metal oxide due to high activation energy. It can be concluded that Sb_2O_5 (Sb^{+5}) doped on SAPO-34 is responsible for propylene, butylenes and benzene formation. Sb_2O_3 (Sb^{+3}) loaded on SAPO-34 governs the oxygenates formation, which the result is similar to when using unsupported pure Sb_2O_3 and Sb_2O_5. However, due to the interaction between the metal oxides and the support, highly dispersed Sb_2O_5 (Sb^{+5}) observed at calcination temperature of 400 °C enhances the oil yield and the formation of bigger hydrocarbons rather than benzene.

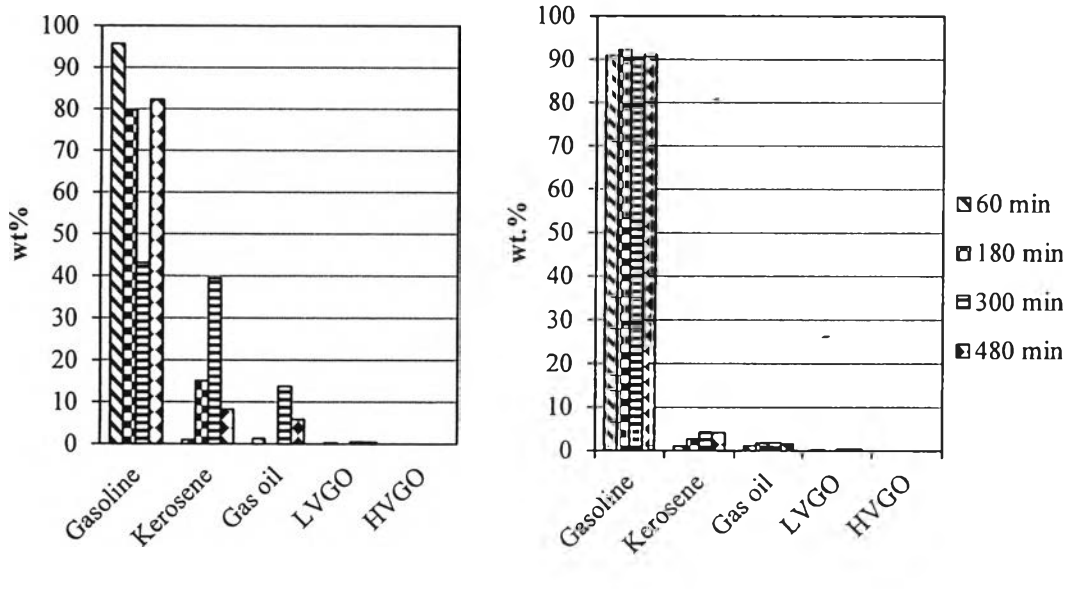

Figure 4.63 Petroleum fractions in oils from using 7 wt. % antimony oxide-doped SAPO-34 catalysts calcined at 400 °C (left) and 700 °C (right).

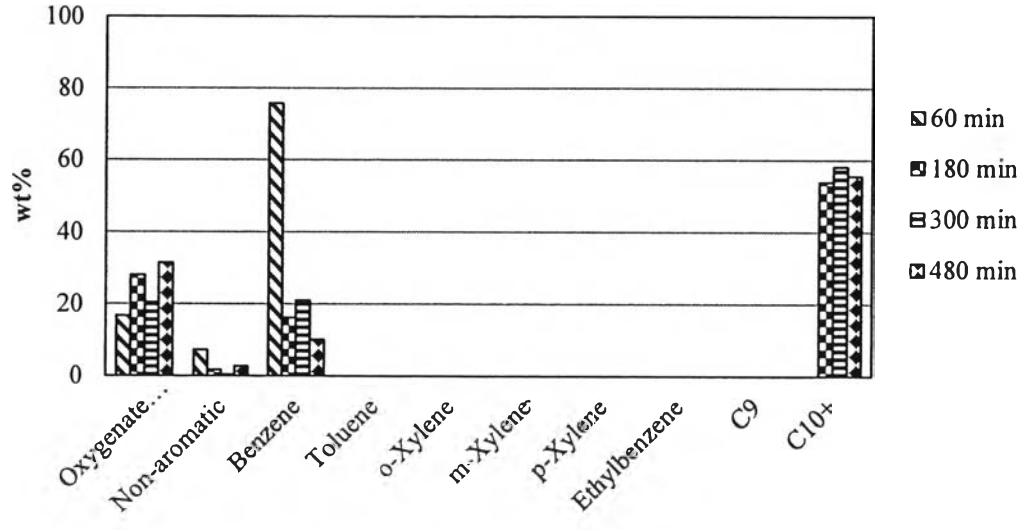

Figure 4.64 Composition of oils from 7 wt.% of antimony oxide-loaded SAPO-34 calcined at 400 C°.

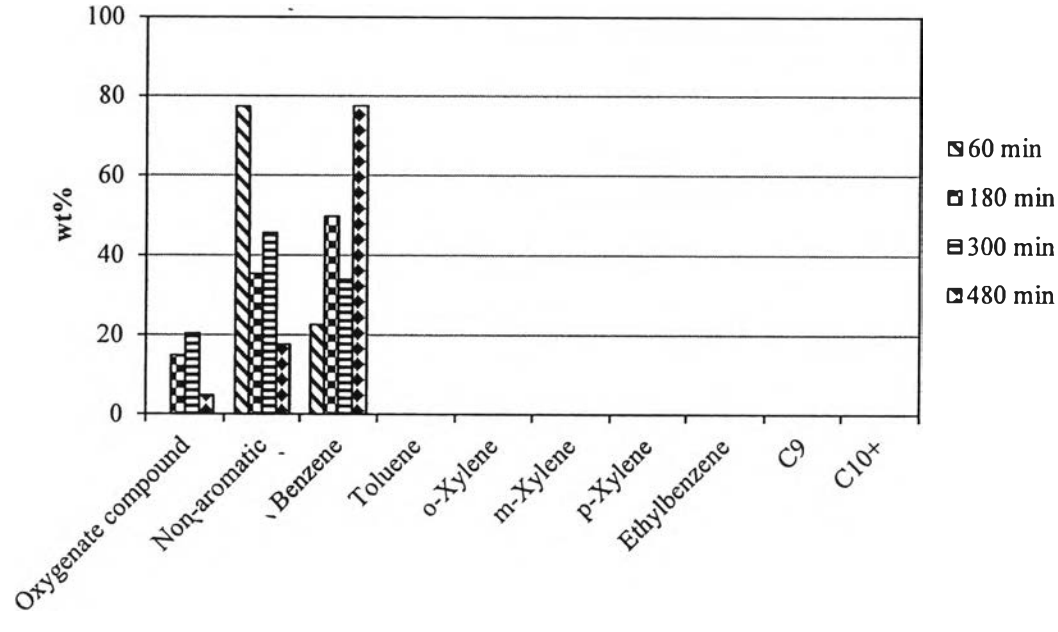

Figure 4.65 Composition of oils from 7 wt.% of antimony oxide-loaded SAPO-34 calcined at 700 C°.